2008-12-04

$$d = \lambda / 2n \sin \theta$$

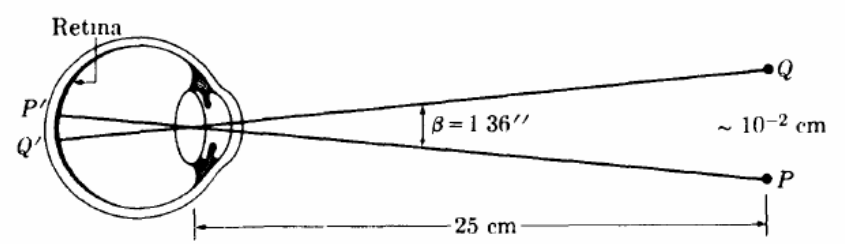

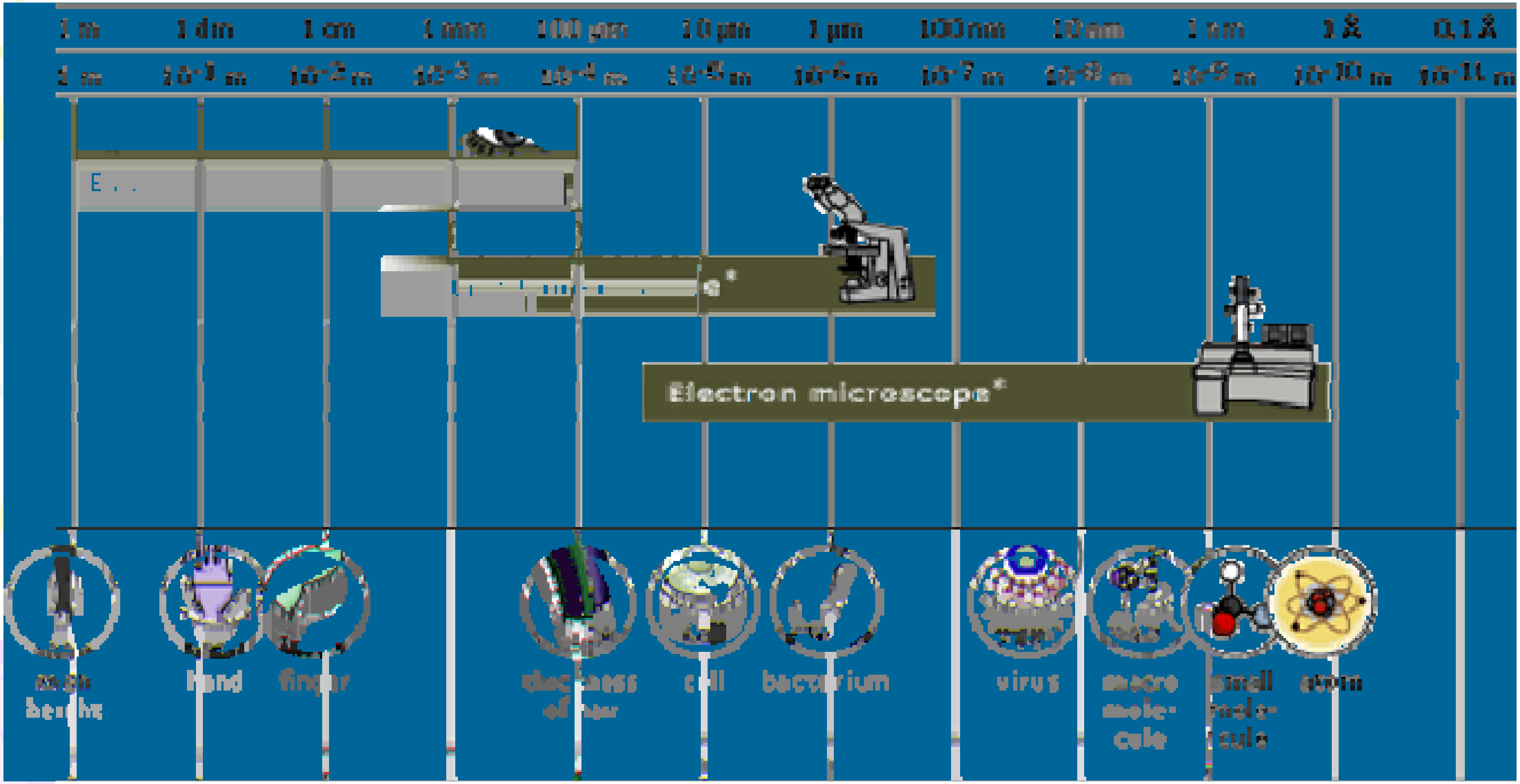

TEM

In situ

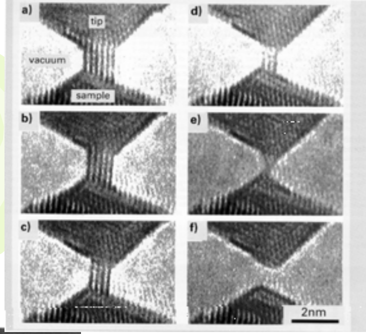

SAED

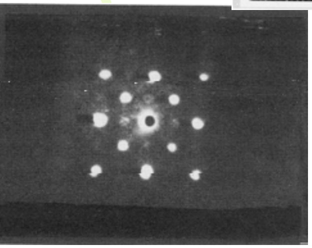

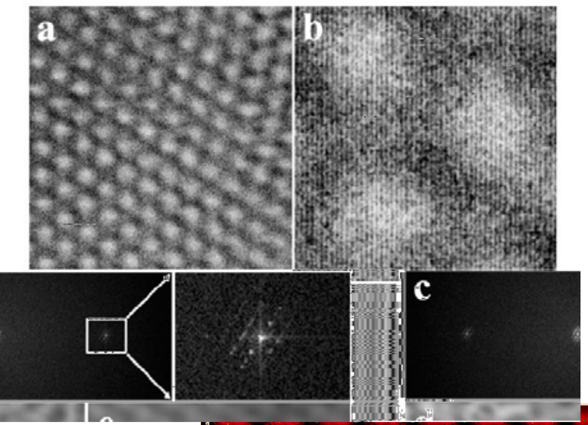

EH

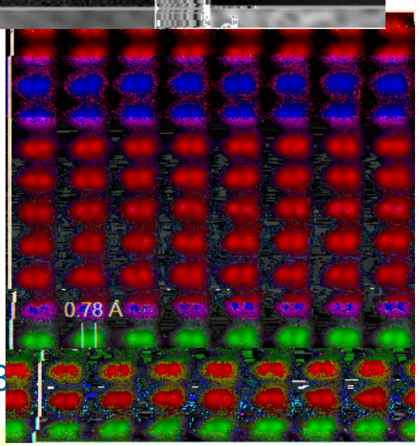

HREM

2008

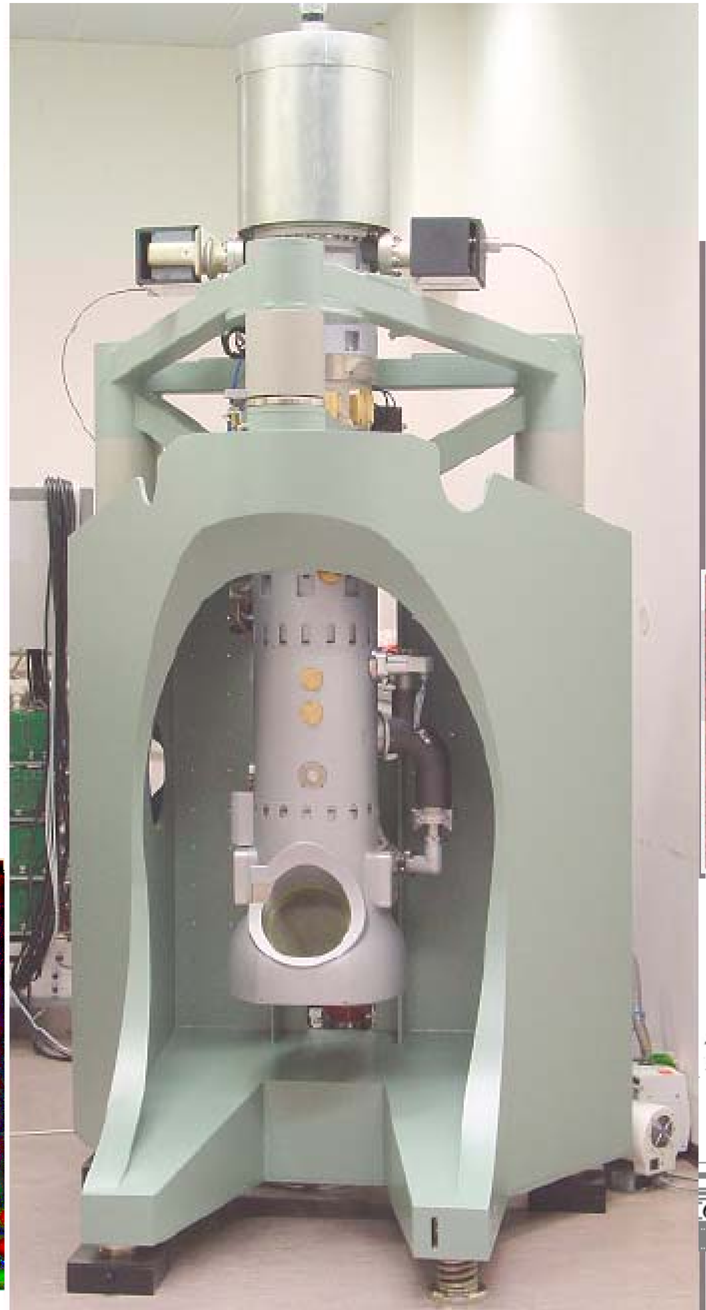

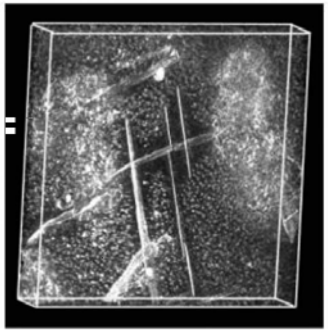

3D

CBED

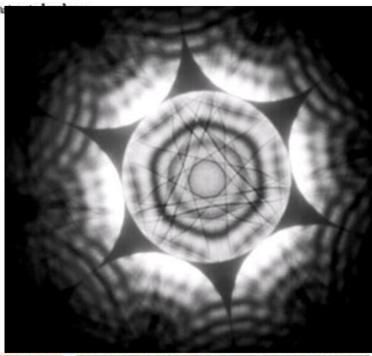

EDX

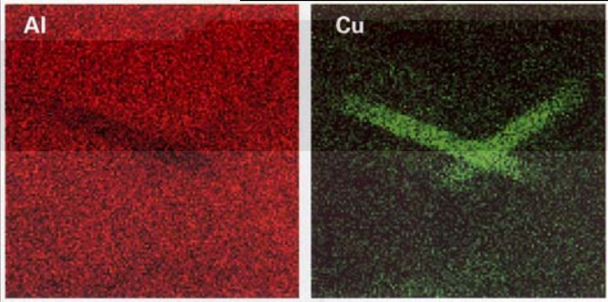

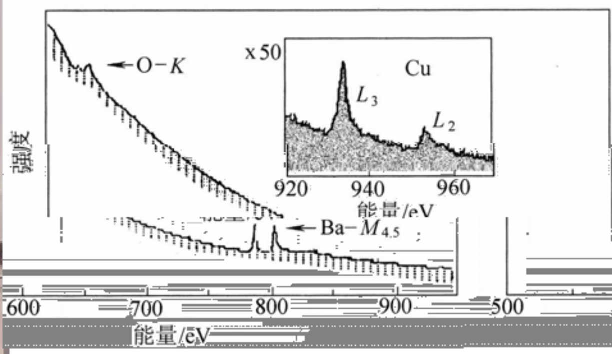

EELS

$d = \lambda/3$, 300

0.0197

0.068

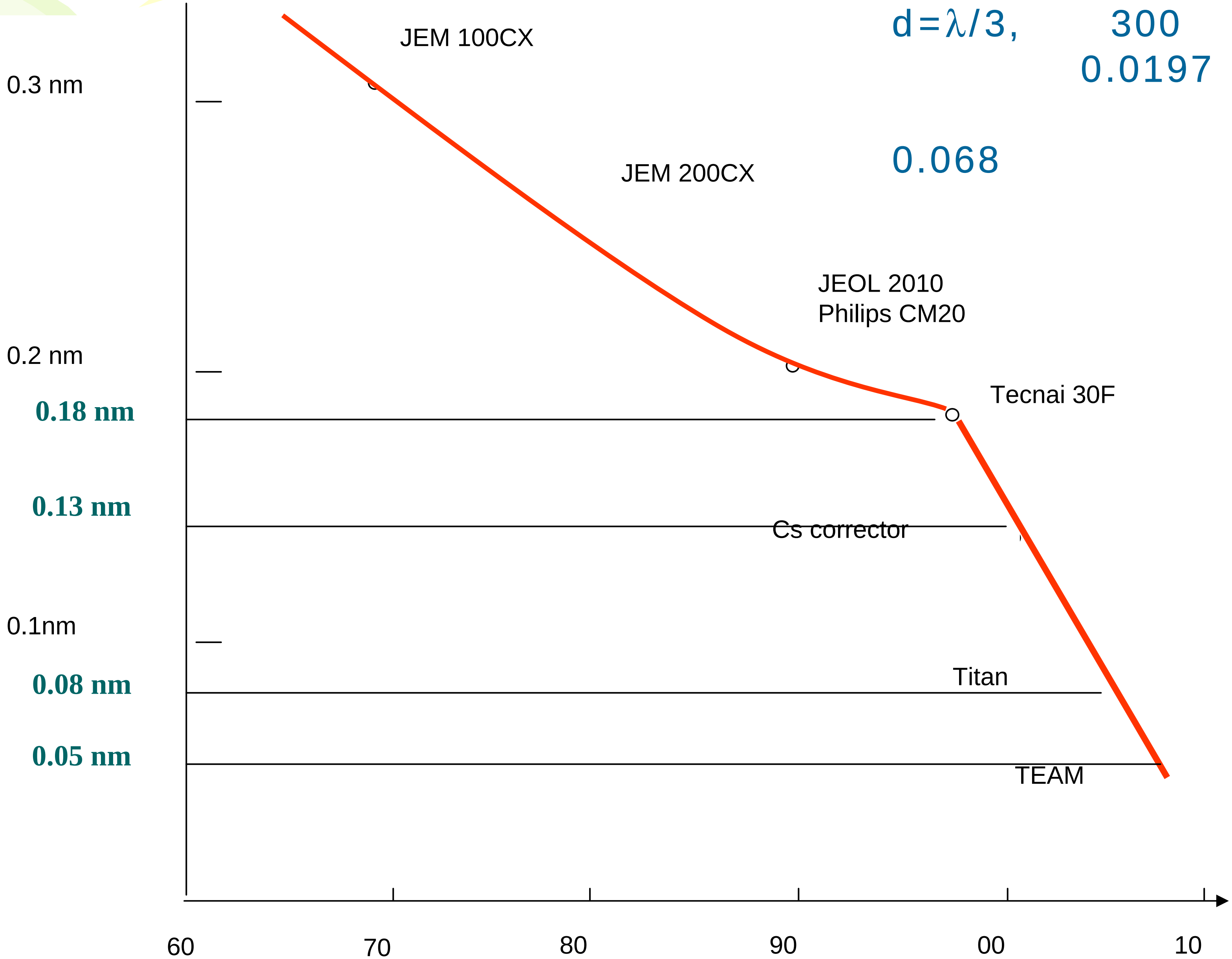

- M.Haider, H.Muller, S.Uhlemann, J.Zach, U.Loebau, and R.Hoeschen: “Prerequisites for a Cc/Cs-corrected ultrahigh-resolution TEM”, Ultramicroscopy 108 (2008) 167.
- O.L.Krivanek, G.J.Corbin, N.Dellby, B.F.Elson, R.J.Keyse, M.F.Murfitt, C.S.Own, Z.S.Szilagyi, J.W.Woodruff: “An EM for the aberration-corrected era”, Ultramicroscopy 108 (2008) 179.
- M.A.O’Keefe: “Seeing atoms with aberration-corrected sub-ÅngstrÖm EM”, Ultramicroscopy 108 (2008) 196.
- H.H.Rose: “Optics of high-performance EM”, Sci. Tech. Adv. Mat., 9 (2008) 014107.

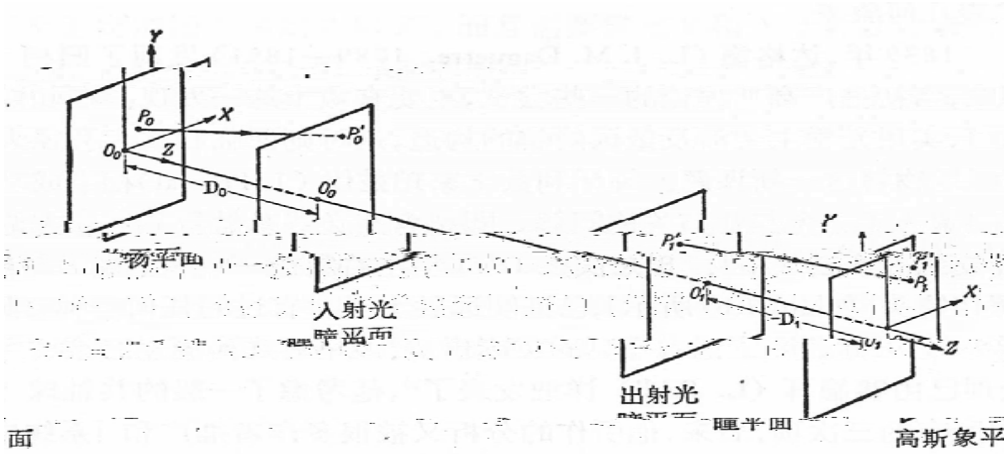

•

P^*_1 P_0

P_1 $\overrightarrow{P_1^* P_1}$

- **n** **n**
M
T
M **TC** **r**

θ,ϕ,ϕ’

- ϕ θ
ϕ θ
ϕ ϕ

5

•

$$\sin\theta = \theta - \frac{\theta^3}{3} + \cdots$$

$$\frac{n}{s} + \frac{n'}{s'} = \frac{n' - n}{r}$$

5

L.Seidel **[L. Seidel. Astr. Nachr., 43(1856), No.1027,289, No.1028,305, No.1029,321.]**

(Seidel sums)

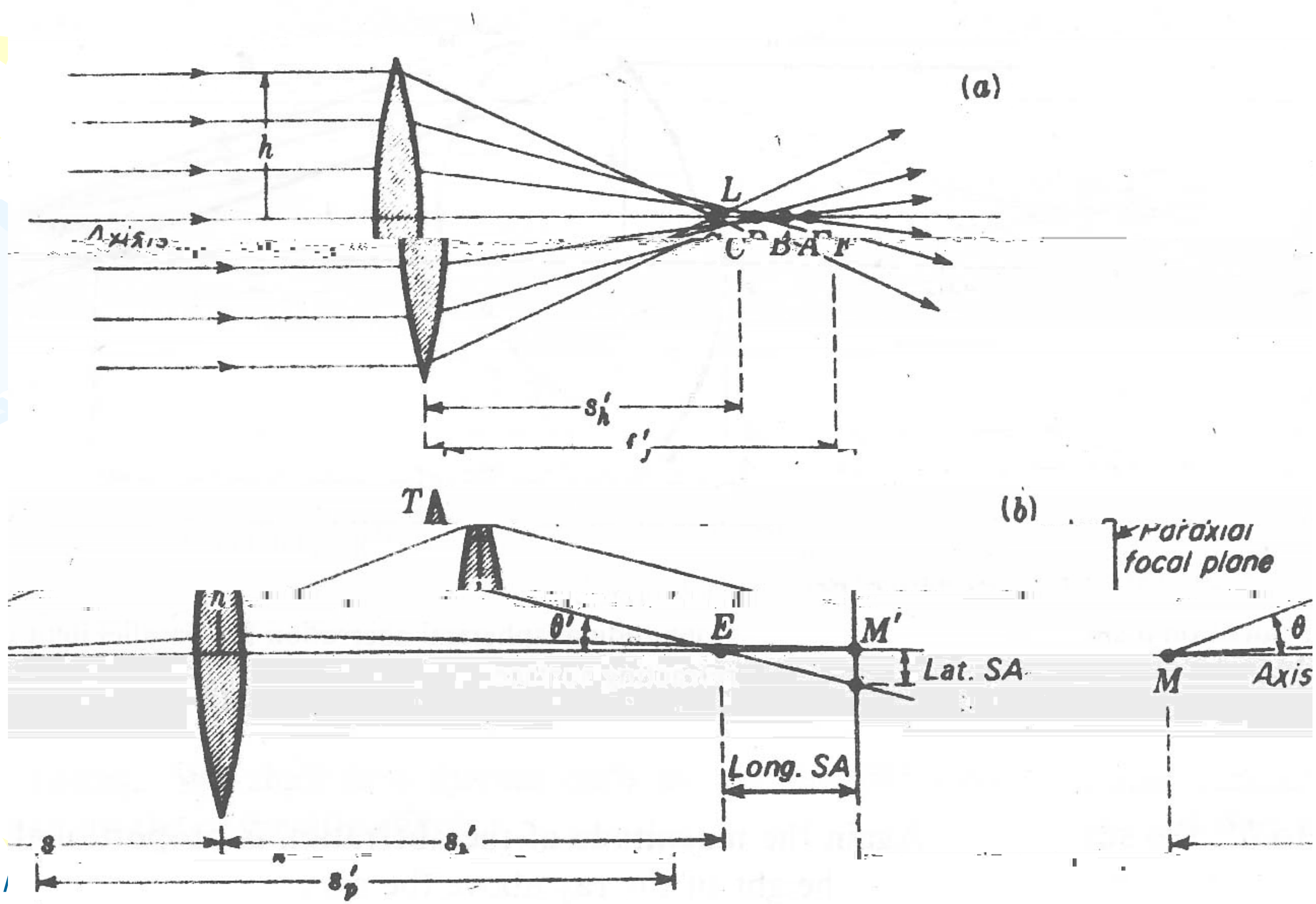

(a)
h
L
C B A F
s_h'
f_j'
(b)
T
Paraxial focal plane
θ'
E
M'
Lat. SA
θ
M
Axis
Long. SA
s
s_h'
s_p'

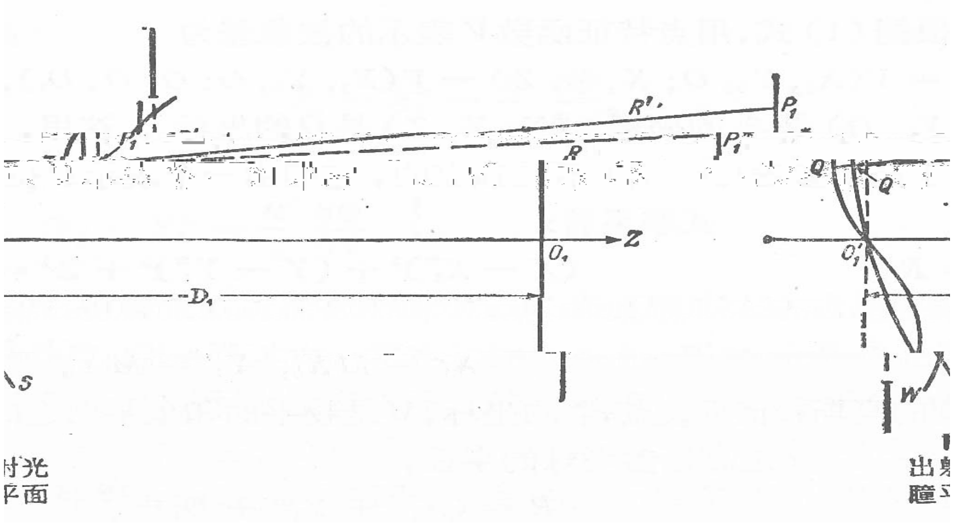

- $\bar{Q}$ O_1' $[P_1\bar{Q}]=[P_1O_1']$

$$\Phi=[P_1Q]-[P_1O'_1]$$

- **x_0,y_0,0 P_0** X,Y,Z **Q**

X_0X+Y_0Y **,** $x_0^2+y_0^2,\ X^2+Y^2$

- (Max Born & Emil Wolf: << Principles of Optics>> (5th ed.) Pergamon Press, 1975.

1978)

$$\Phi = c(x_0^2 + y_0^2) + \Phi^{(4)} + \Phi^{(6)} + \cdots$$

- $\gamma^2 = x_0^2 + y_0^2$, $\rho^2 = X^2 + Y^2$, $\kappa^2 = x_0 X + y_0 Y$
- 4

$$\Phi^4 = -\frac{1}{4} A\gamma^4 - \frac{1}{4} B\rho^4 - C\kappa^4 - \frac{1}{2} D\gamma^2\rho^2 + E\gamma^2\kappa^2 + F\rho^2\kappa^2$$

- $-\frac{1}{4} A\gamma^4$

B-

C- **D-** **E-** **F-**

-

, $\chi(\vec{r})$, $\chi(\vec{g})$, $\chi(\theta)$

- $$\phi = c(x_0^2 + y_0^2) + \frac{1}{4}B\rho^4 \qquad \rho^2 = X^2 + Y^2$$,
- , $$\chi(\vec{g}) = \frac{1}{2}\Delta f \lambda^2 |\vec{g}|^2 + \frac{1}{4} C_s \lambda^4 |\vec{g}|^4$$
- , $$\chi(\theta) = \frac{1}{2}\theta\tilde{\theta}C_1 + \frac{1}{4}(\theta\tilde{\theta})^2 C_3$$

- **sin**

- C_1(nm)； A_1(nm)； A_2(nm)； B_2 nm ； C_3,C_s(m)；
- A_3(m); S_3(m); A_4(m); B_4(m); D_4(m);
- C_5(mm); A_5 mm ; R_5(mm); S_5(mm); A_6(mm);
- B_6 mm ; D_6(mm); F_6 mm ; C_7 mm

-
-
- [Lord Rayleigh: Phil. Mag., (5)8 (1879), 463.]

1/4 **20%**

1/4

•

•

1/4 100 nm

0.3m/100nm=3 10^6

2.5m/100nm=2.5 10^7

• VG HB501 STEM

40 m /4 1pm

40 m/1pm=4 10^7; STEM

100 m

100 m/1pm=1 10^8

1.6-4

•

(O.L.Krivanek, P.D.Nellist, N.Dellby, M.F.Murfitt, and Z.Szilagyi: Ultramicroscopy 96 (2003) 229.)

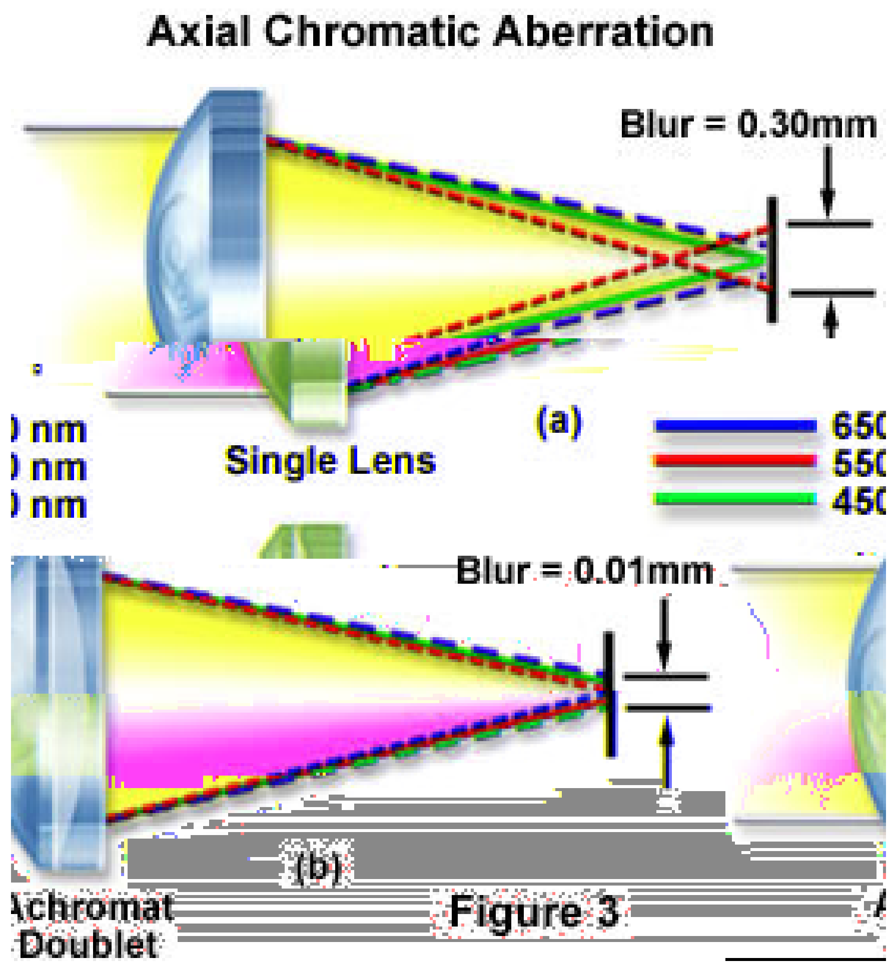
Axial Chromatic Aberration
Blur = 0.30mm
(a)
Single Lens
Blur = 0.01mm
(b)
Doublet
Figure 3

Sample

Lens

Diffraction Pattern

Image

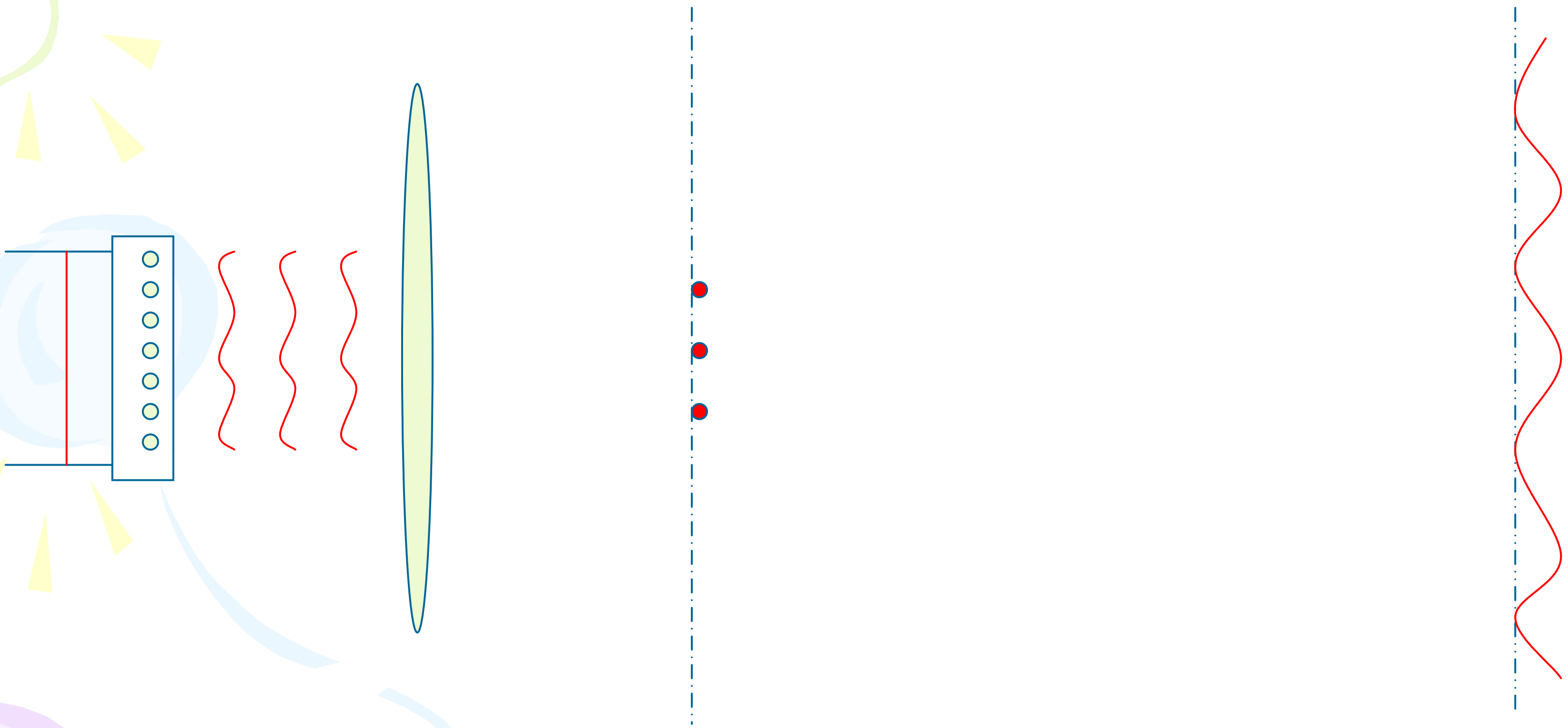

Plane

Modified by sample

Modified by lens

Image reconstruction

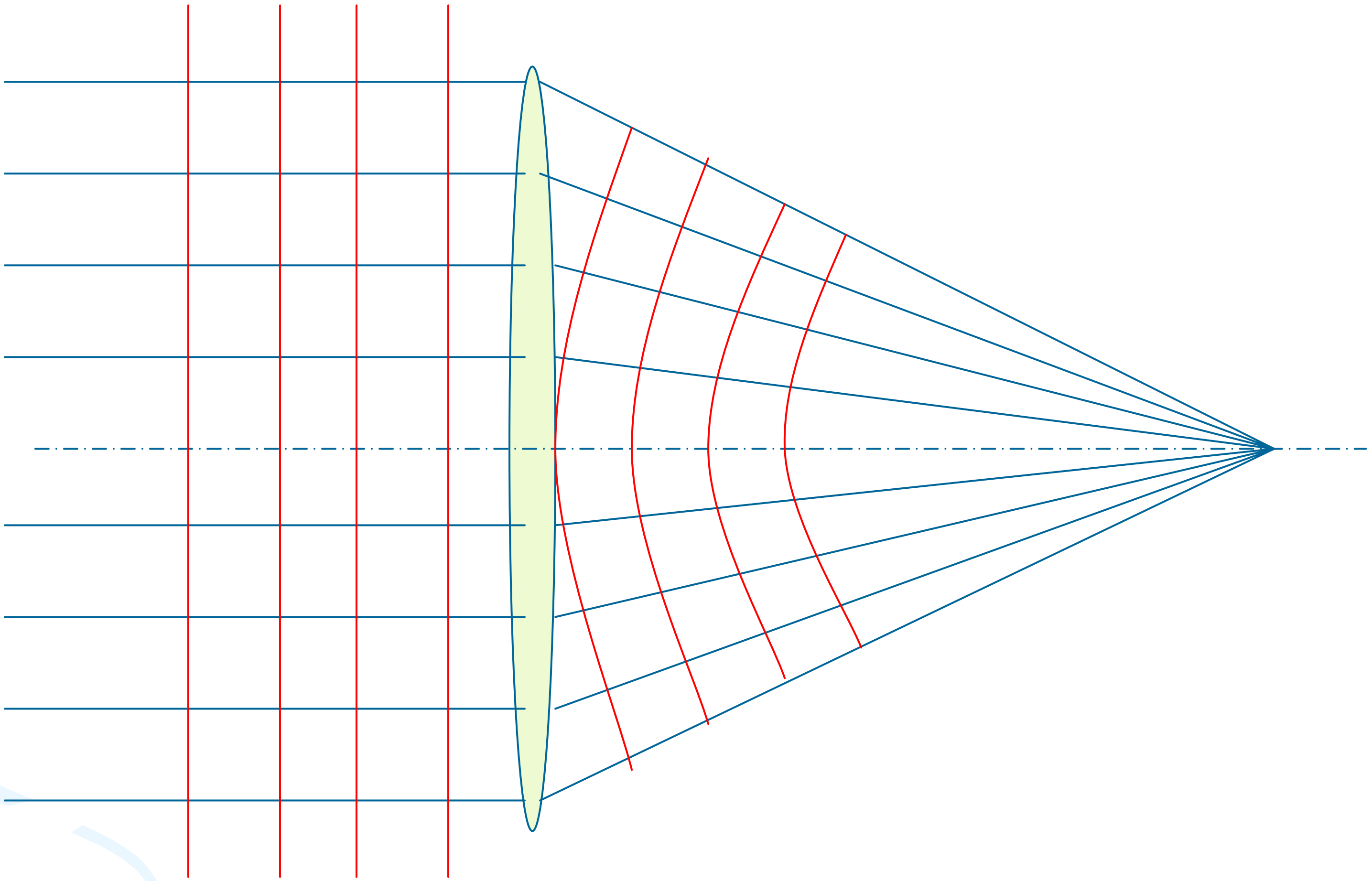

O.Scherzer

(J.Appl. Phys. 20,20, 1949)

$$\chi=\pi[0.5C_s\lambda^3(u^2+v^2)^2+\Delta f\lambda(u^2+v^2)]$$

- C_s—
  λ——
  Δ —
-

,

$$I(g) \sim |A(g)|^2 |E(g)|^2 |\sin\chi(g)|^2 |Q_p(g)|^2$$

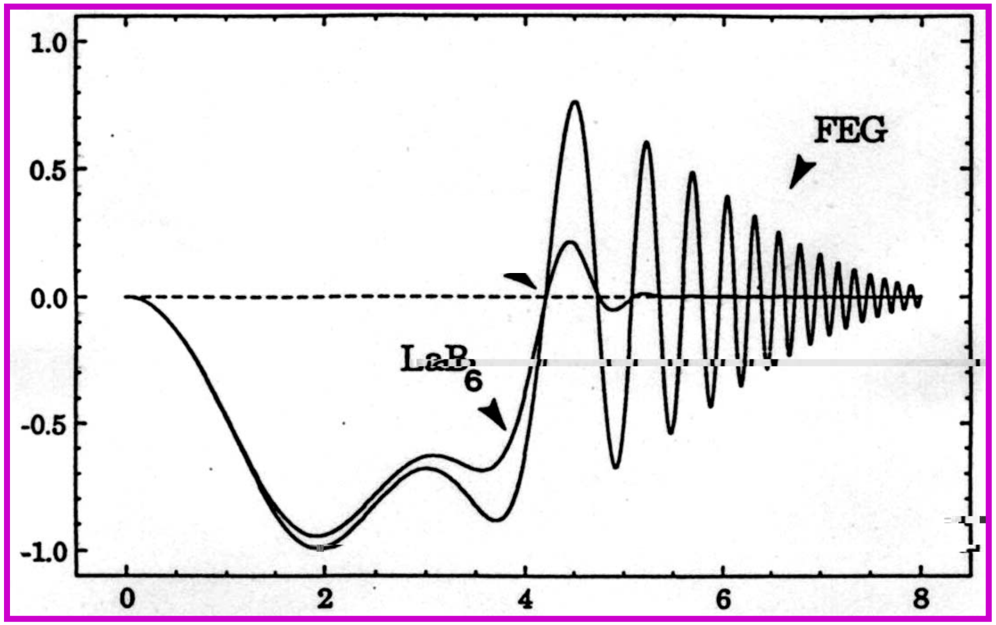

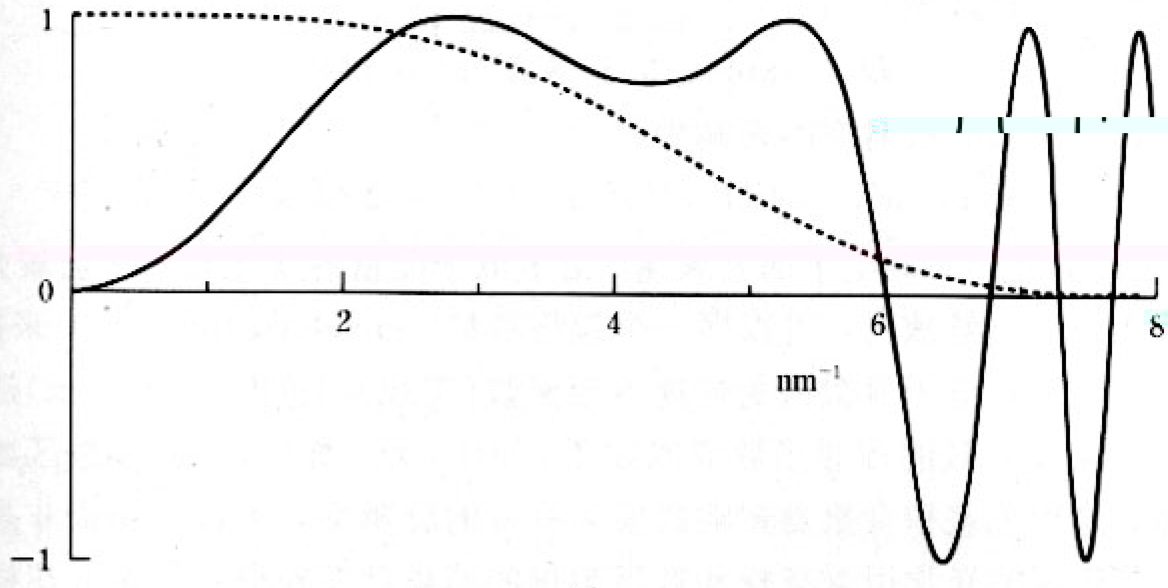

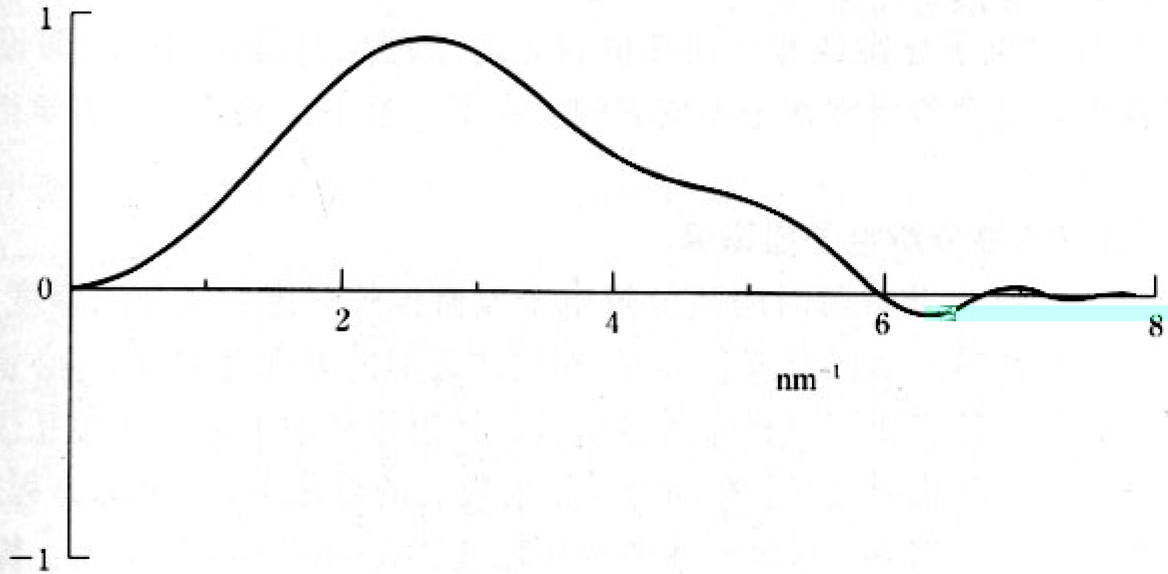

$$d_s = 0.67\, C_s^{1/4} \lambda^{3/4}$$

— A_2

$$\chi(\mathbf{u}) = \pi \varepsilon \lambda |\mathbf{u}|^2 + \pi C_S \lambda^3 |\mathbf{u}|^4 / 2$$

[illegible]

Limits from three-fold astigmatism $|A_2|$[a]

$\|A_2\|$ (μm)	χ at 2 Å	χ at 1 Å	$d_{\pi/4}$ (Å)
2.25	0.73π	5.81π	2.85
1.0	0.33π	2.58π	2.18
0.5	0.16π	1.29π	1.73
0.2	0.065π	0.52π	1.27
0.1	0.033π	0.26π	1.01
0.05	0.016π	0.13π	0.80
0.03	0.010π	0.08π	0.68

[a] Contribution to lens phase change $\chi(\mathbf{u})$ from three-fold astigmatism $|A_2|$ at spacings of 2 and 1 Å, and the spacing $d_{\pi/4}$ at which phase change from three-fold astigmatism reaches $\pi/4$ at 300 keV. Uncorrected value of $|A_2|$ for the NCEM CM300FEG/UT is 2.25 μm. Measurements of corrected values of $|A_2|$ gave means of 0.05 and 0.03 μm.

[110]

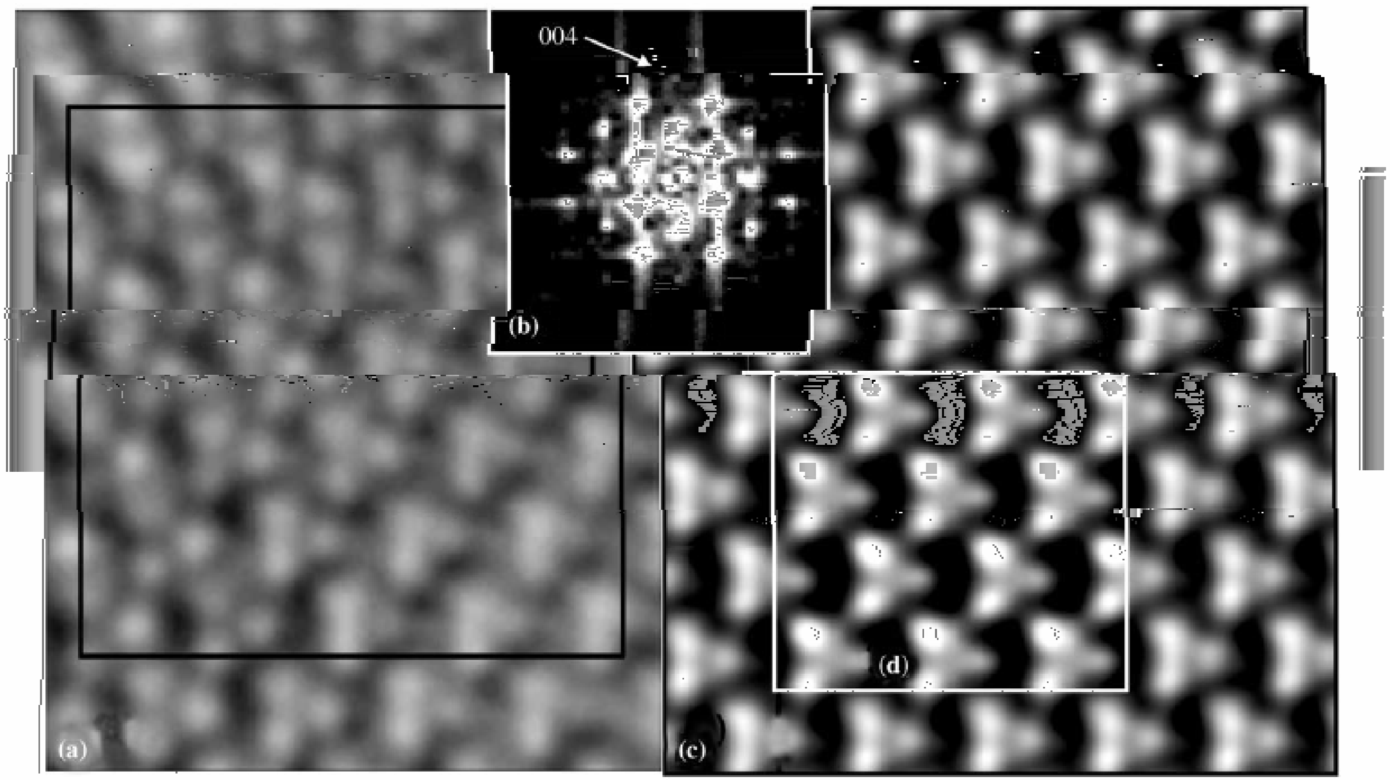

Fig. 8. (a) Experimental OÅM image of CVD diamond before correction of three-fold astigmatism. (b) Diffractogram shows specime orientation is [1 1 0], with strong 1 1 1 and 113 spots, weak 220 and 331 spots, and very weak 004's (arrowed). (c) Averaging (p1 : Crisp™) shows white spots separated by approximately $|\mathbf{a}|_{diamond}/4$, but with extra spots producing triangular white clusters. (d) Imag simulated from diamond [1 1 0] match best at $|A_2| = 2.25\,\mu m$.

A_2

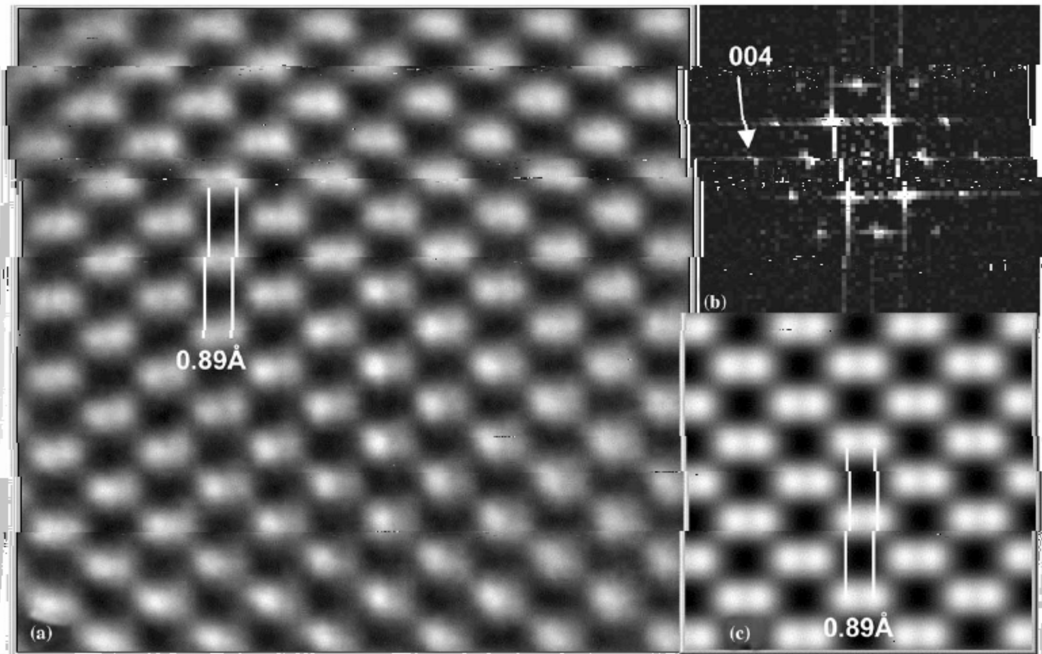

Fig. 10. (a) Experimental OÅM image of CVD diamond in [110] orientation after correction of three-fold astigmatism to below ... 0.05µm. (b) Diffractogram shows a strong 004 presence (arrowed) ... "dumbbell" images with 0.89 ...

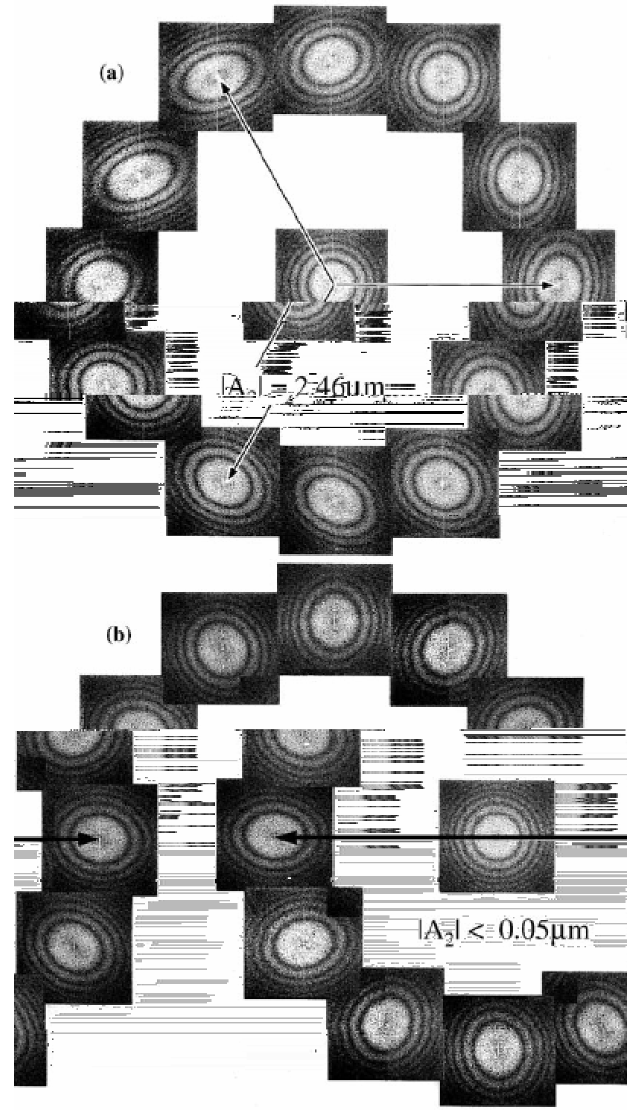

tilt series of diffractograms from a thin ecimen. (a) Strong three-fold astigmatism .46 µm before correction shows distinct rrowed). (b) Corrected series measured at pses pointing to the tilt origin.

Fig. 9. OAM "clock" amorphous carbon sp measured at $|A_2| = 2$ three-fold character (a 0.05 µm shows all elli

M.A. O'Keefe et al., Ultramicroscopy 89 (2001) 215–241

$$d_{A_2} = 1/|\mathbf{u}|_{A_2} = (8A_2\lambda^2/3)^{1/3}$$

$A_2 = 3/8u^3\lambda^2$

List of the upper limits with respect to the $\pi/4$ criterion of all axial aberrations considering only one particular aberration coefficient

Aberration	80 kV	120 kV	200 kV		300 kV
	80 pm	65 pm	100 pm	50 pm	50 pm
Focus C_1 (nm)	0.40	0.31	1.0	0.25	0.4
Two-fold astigmatism A_1 (nm)	0.40	0.31	1.0	0.25	0.4
Three-fold astigmatism A_2 (nm)	11.50	9.2	60.0	7.5	13
Second-order coma B_2 (nm)	3.80	3.1	20.0	2.5	5.0
Third-order spherical aberr. C_3 (μm)	0.30	0.24	3.2	0.2	0.5

•

M. Haider, H. Muller, S. Uhlemann, J. Zach, U. Loebau, R. Hoeschen:Ultramicroscopy 108 (2008) 167–178

$$I(g) \sim |A(g)|^2 |E(g)|^2 |\sin \chi(g)|^2 |Q_p(g)|^2$$

•

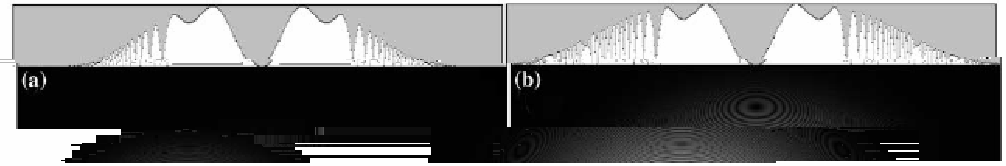

sin

•

M.A. O'Keefe et al., Ultramicroscopy 89 (2001) 215–241

- 234-236

球差系数 C_s 的测定，迄今为止已有几种方法．Kriv- 关于

出的方法被公认是一种简单而巧妙的测试方法．它 anek[3] 提

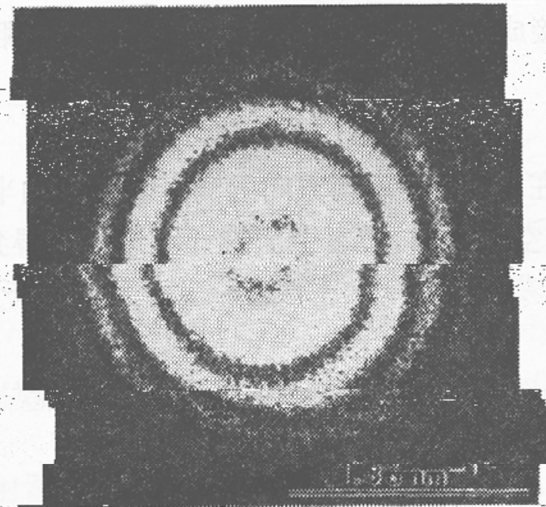

图 6.2　无定形碳膜电子显微象的光学衍射图

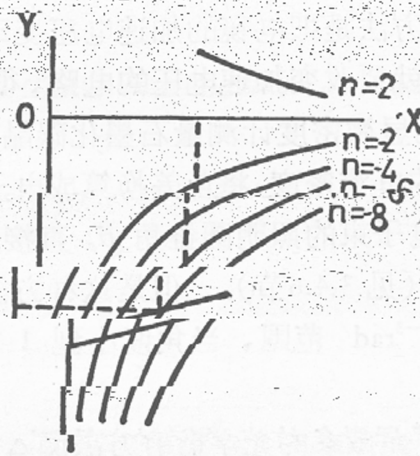

图 6.3　由图 6.2 求解 C_s 及 Δf

如果设 $u^2 = X$，上式可写成联立方程形式

$$\begin{cases} Y = (C_s\lambda^3)X + 2\Delta f\lambda & (6.10) \\ Y = n/X & (6.11) \end{cases}$$

从 X 的一次式和双曲线的交点能求出暗环的空间频率

反之，从图 6.2 的光学衍射图求得明暗环的空间频率，画在图 6.3 上，连接成直线，则直线的斜率是 $C_s\lambda^3$，截距为 $2\Delta f\lambda$，即

$$C_s = 斜率/\lambda^3 \tag{6.12}$$

$$\Delta f = 截距/2\lambda \tag{6.13}$$

[illegible]了准确，在图 6.2 的不同方向上测量明暗环的半径，并换算 [illegible] 为成所对应的空间频率，重复上面的计算过程，得到一系列 C_s [illegible] 和 Δf，再求它们的算术平均值，就得到我们所要测定的 C_s 和 Δf [illegible] 和 Δf。

[illegible] 方向 [illegible] 从一张图各方向的 Δf 值中，取椭圆的长轴与短轴方向的 Δf 值，可以得到象散量

$$C_a = |\Delta f_{\parallel} - \Delta f_{\perp}| \tag{6.14}$$

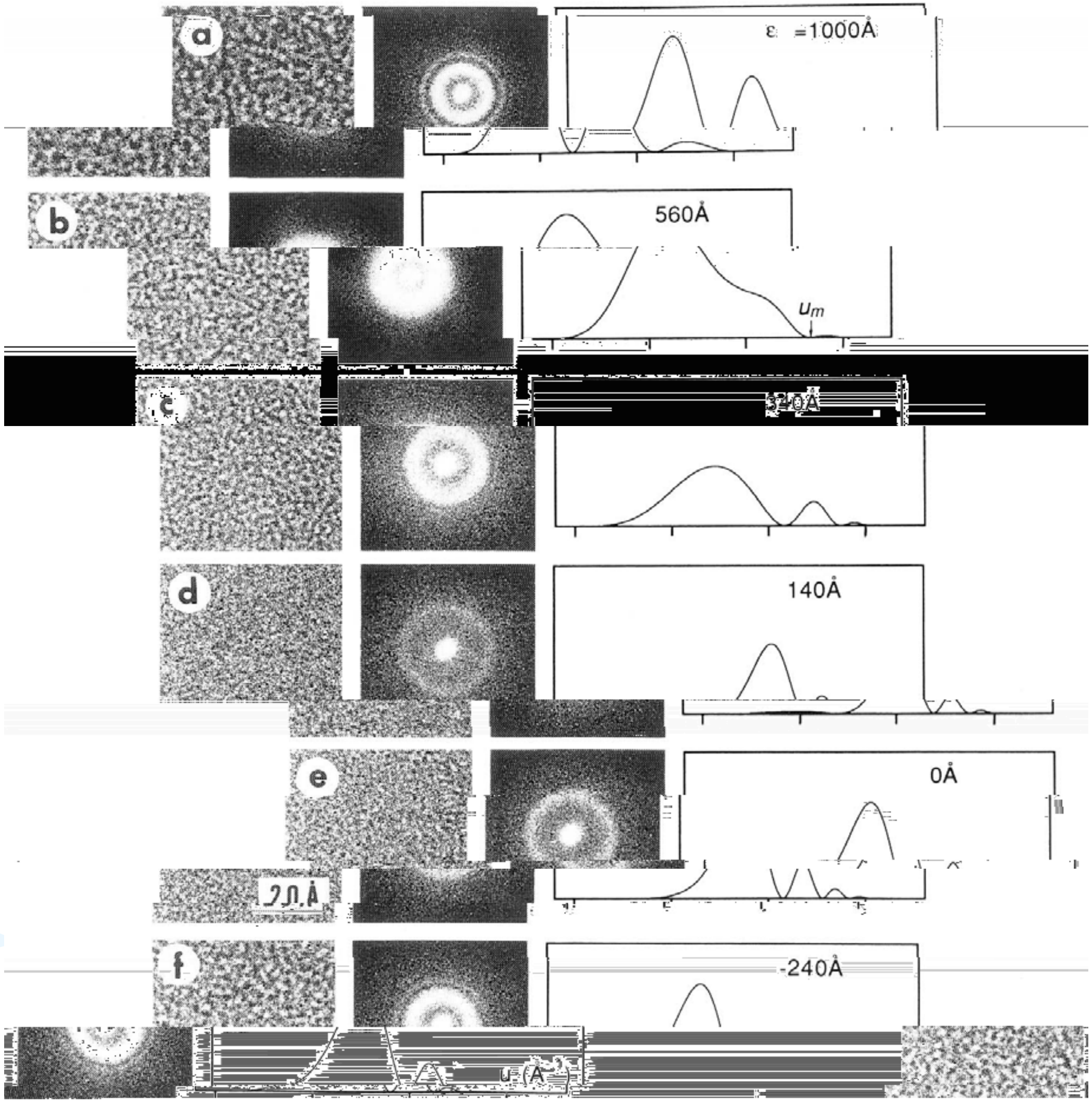

S.Horiuchi:<< Fundamentals of HRTEM>>, North-Holland, 1994, p.223

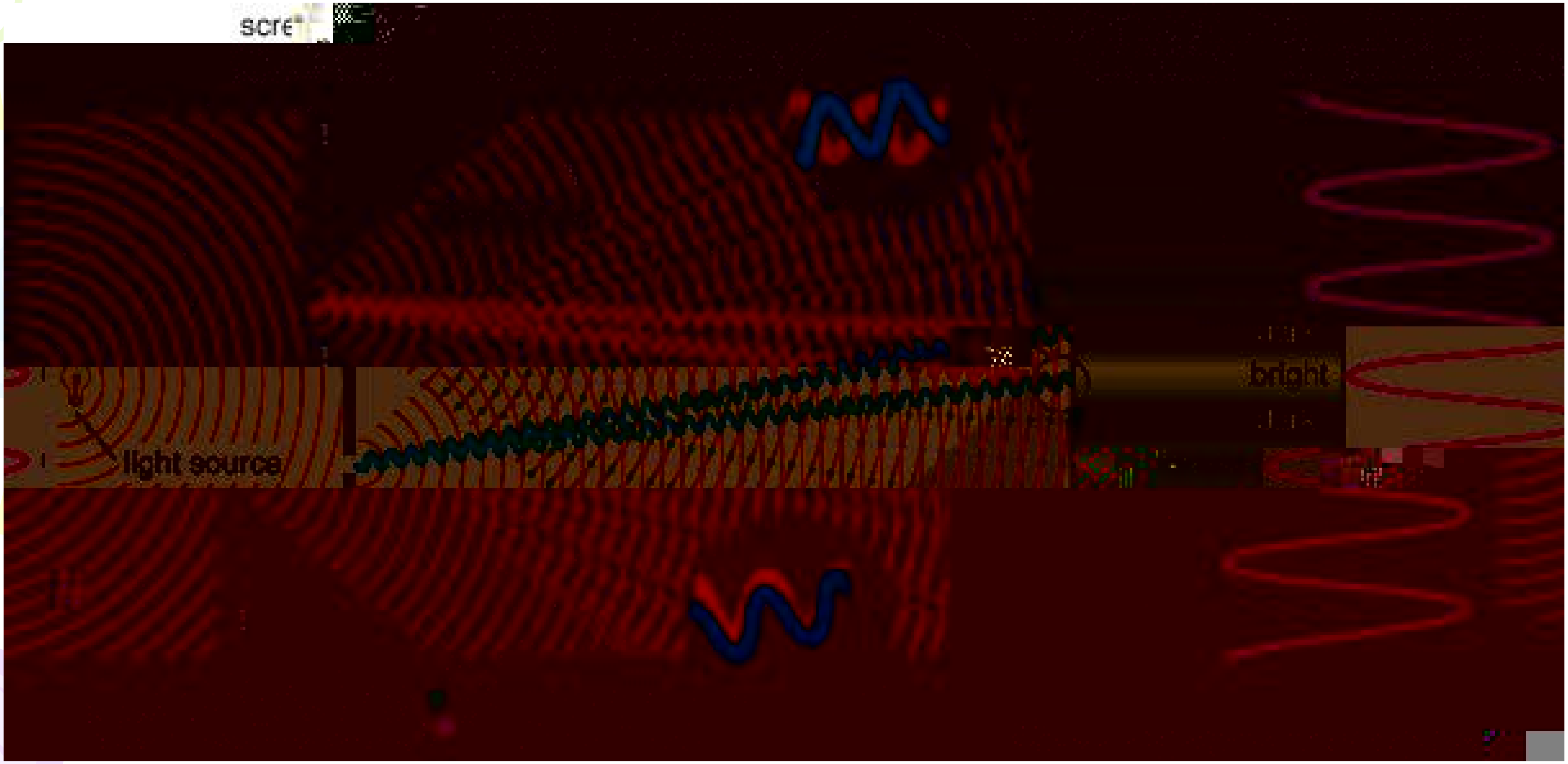
scre
light source
bright

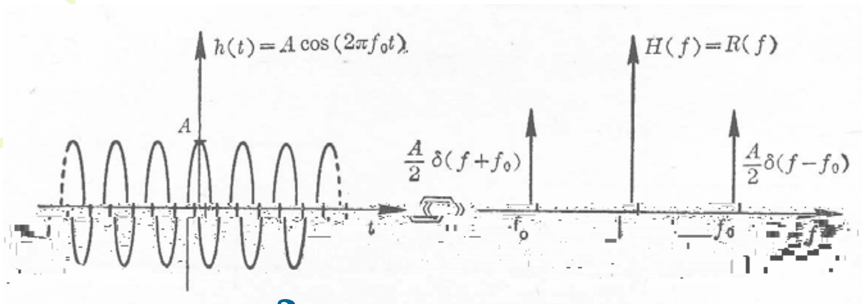

δ

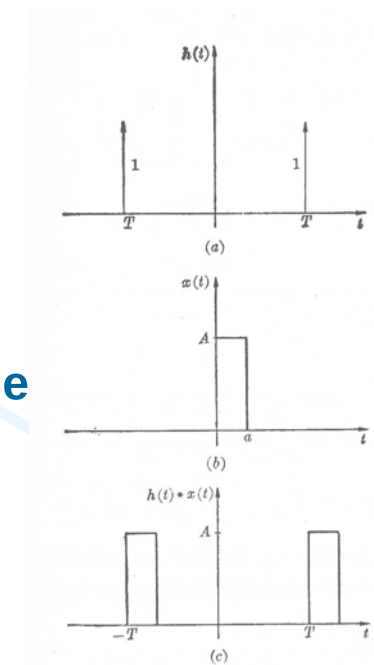

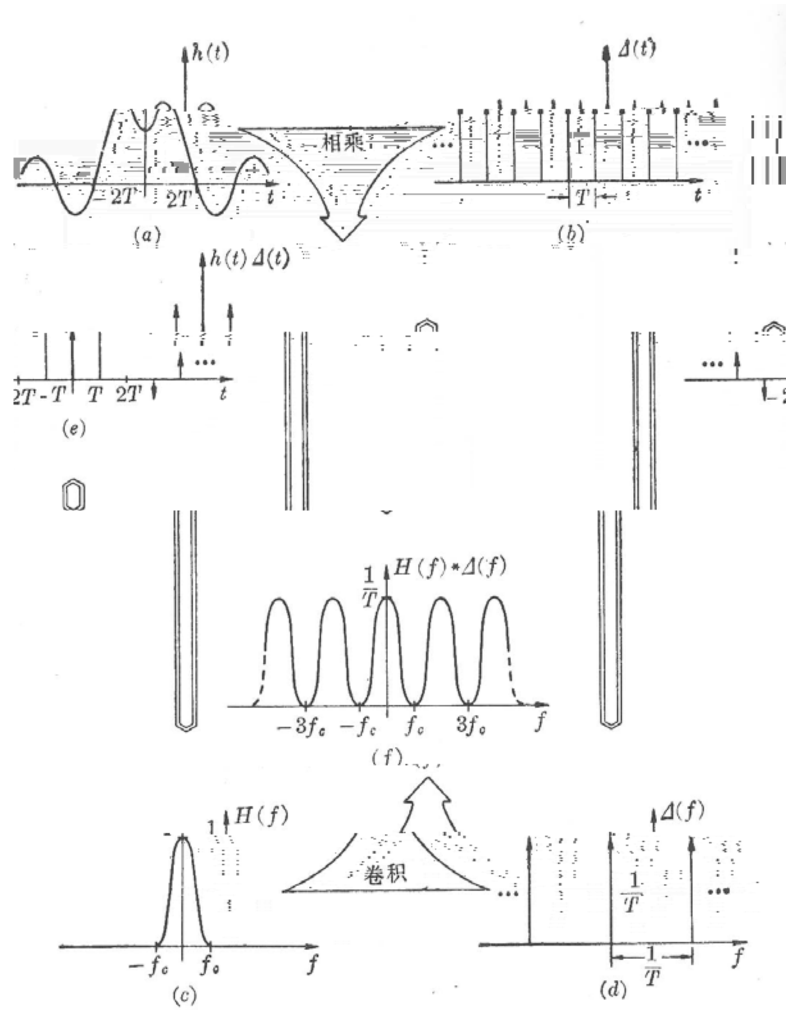

E.O.Brigham: The fast Fourier transform

1979

•

δ

δ

$Q_p = Q'_p(g)Y(g)$ Q'_p

Y δ

A E $\sin\chi$

$$I(g) \sim |A(g)|^2 |E(g)|^2 |\sin\chi(g)|^2 |Q_p(g)|^2$$

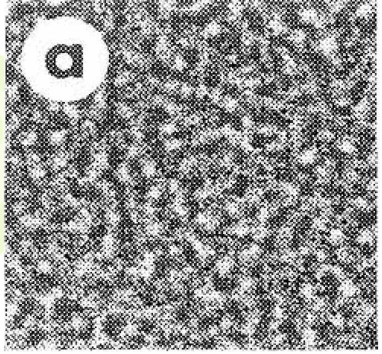

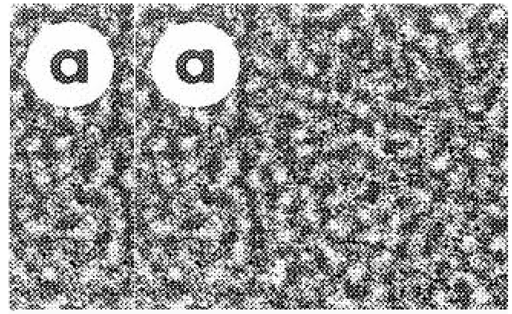

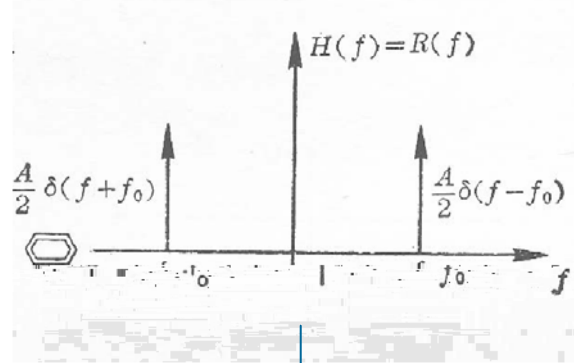

$\mathcal{F}$

$\mathcal{F}$

$\mathcal{F}$

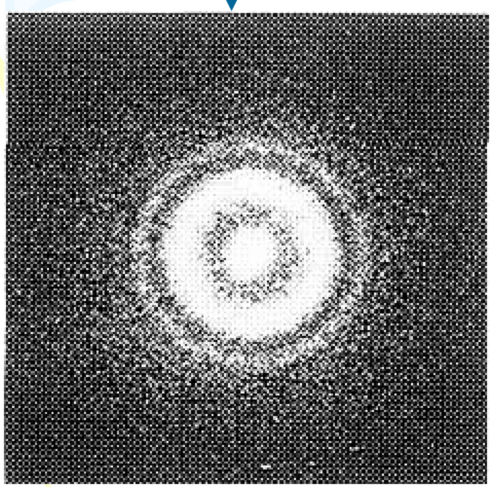

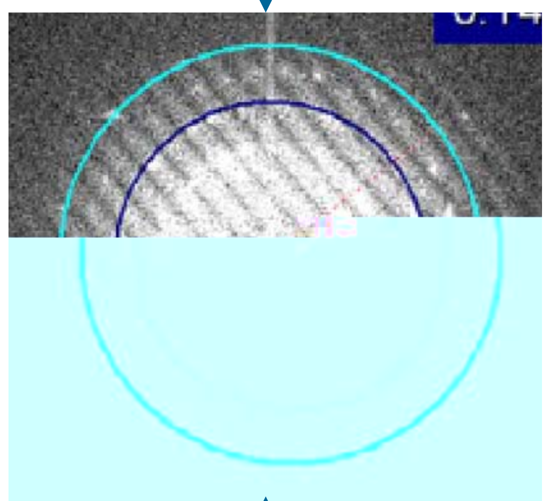

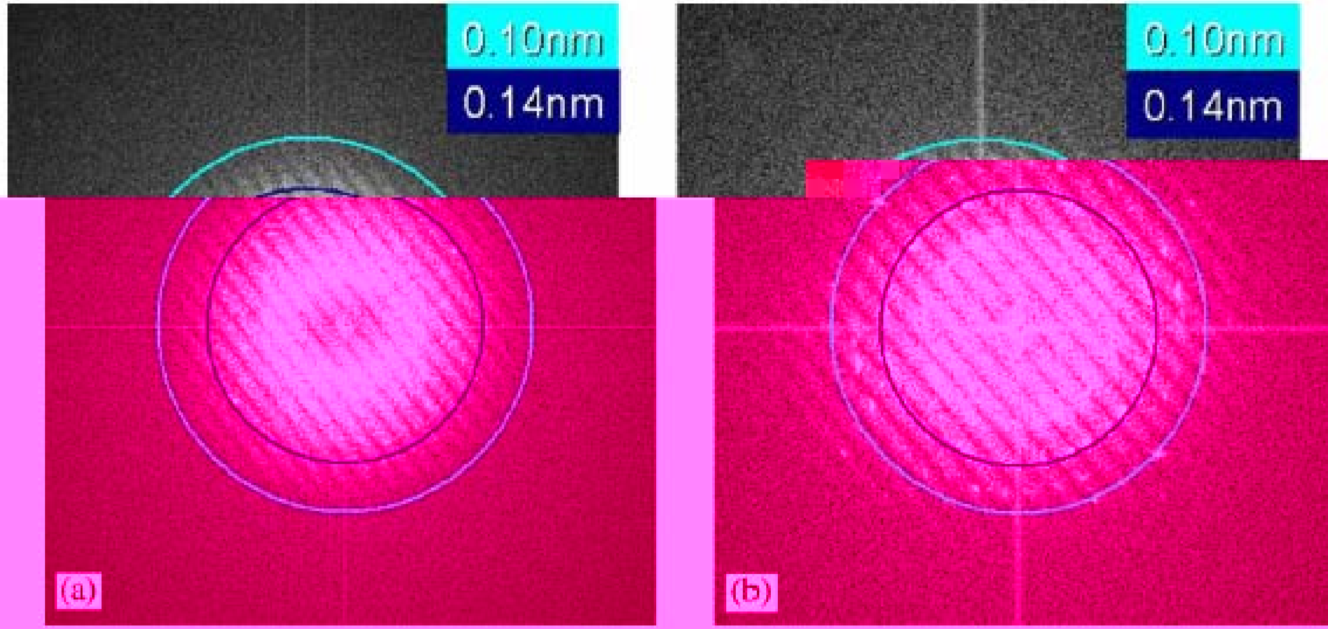

Fig. 2. Two Young fringe images of an amorphous tungsten film, showing the improvement of information limit obtained by t
monochromator: (a) monochromator off ($\Delta E = 0.55$ eV) and Cs corrector [illegible] (b) monochromator on [illegible]
[illegible] Cs corrector on [illegible] The dots in the right image are lattice reflections from small gold particles in the tungsten film u
calibration. The light blue circle shows the 0.10 nm frequency. The dark blue circle shows the 0.14 nm frequency. The Young
show that, without monochromator, the information limit is a little worse than 0.1 nm. With monochromator, the information
well below 0.1 nm. The images were taken with 0.3 nA beam current on the CCD, 1 s exposure time, and 0.2 mrad half conv
angle (a) or 2 mrad half convergence angle (b).

B. Freitag,S. Kujawa,P.M. Mul,J. Ringnalda,P.C. Tiemeijer:Ultramicroscopy 102 (2005) 209–214

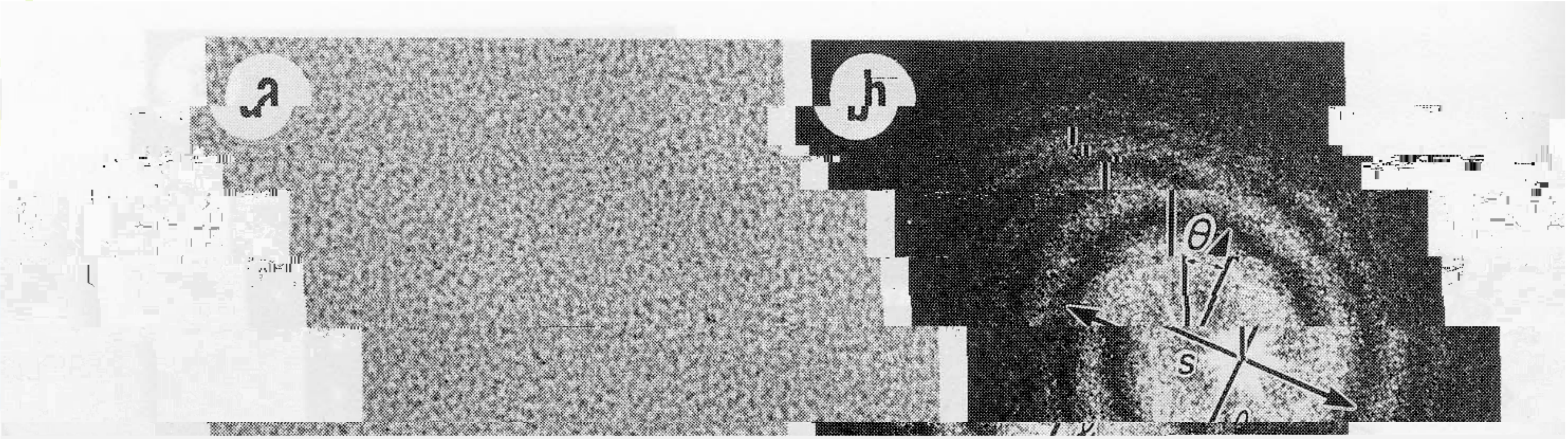

S.Horiuchi:<<Fundamentals of HRTEM>>, North-Holland, 1994, p.224.

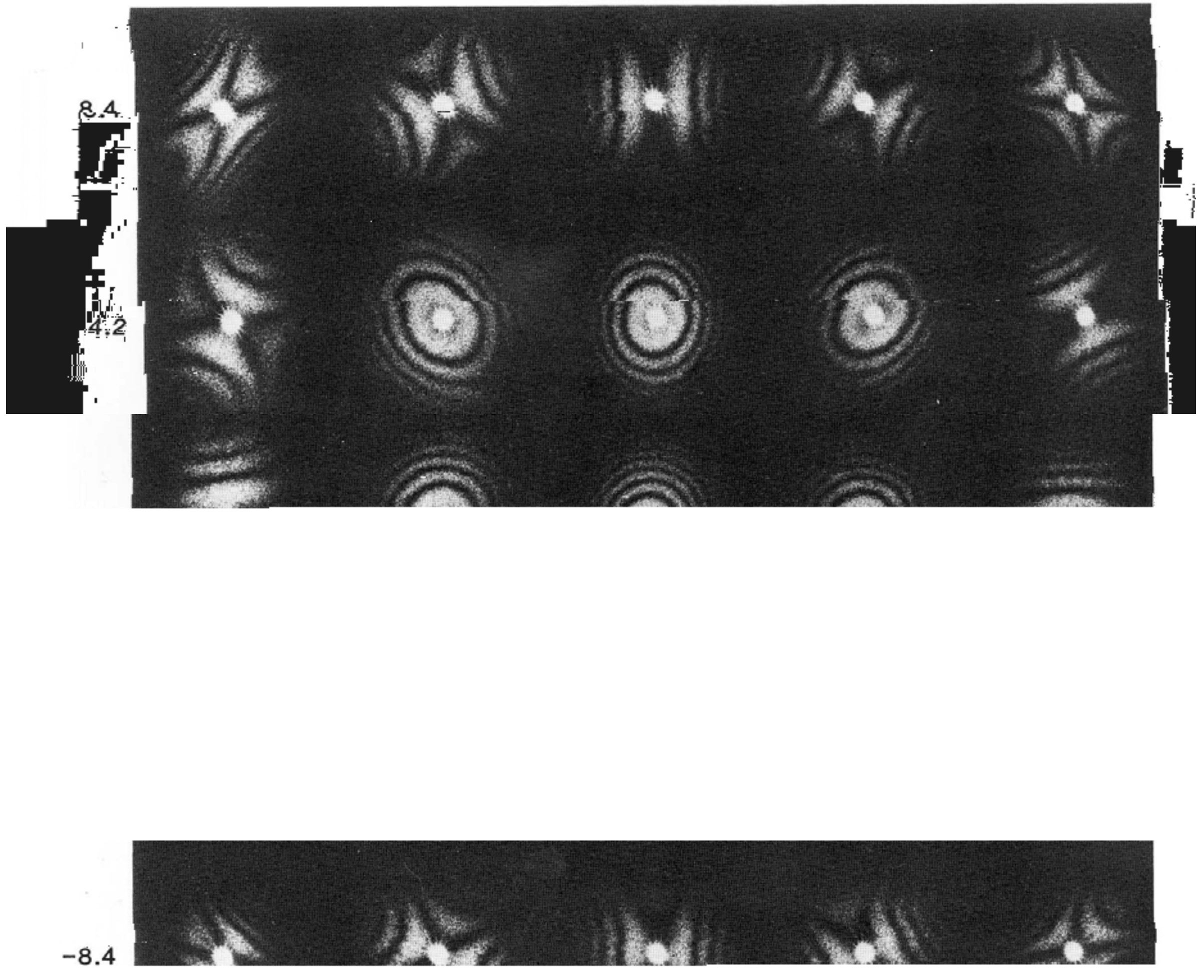

O.L.Krivanek: Chapter 12 <<HRTEM>>, Editors: P.R.Buseck, J.M.Cowley, L. Eyring. Oxford Univ. Press, 1988, pp 546.

- A,B...

C1 A1

-

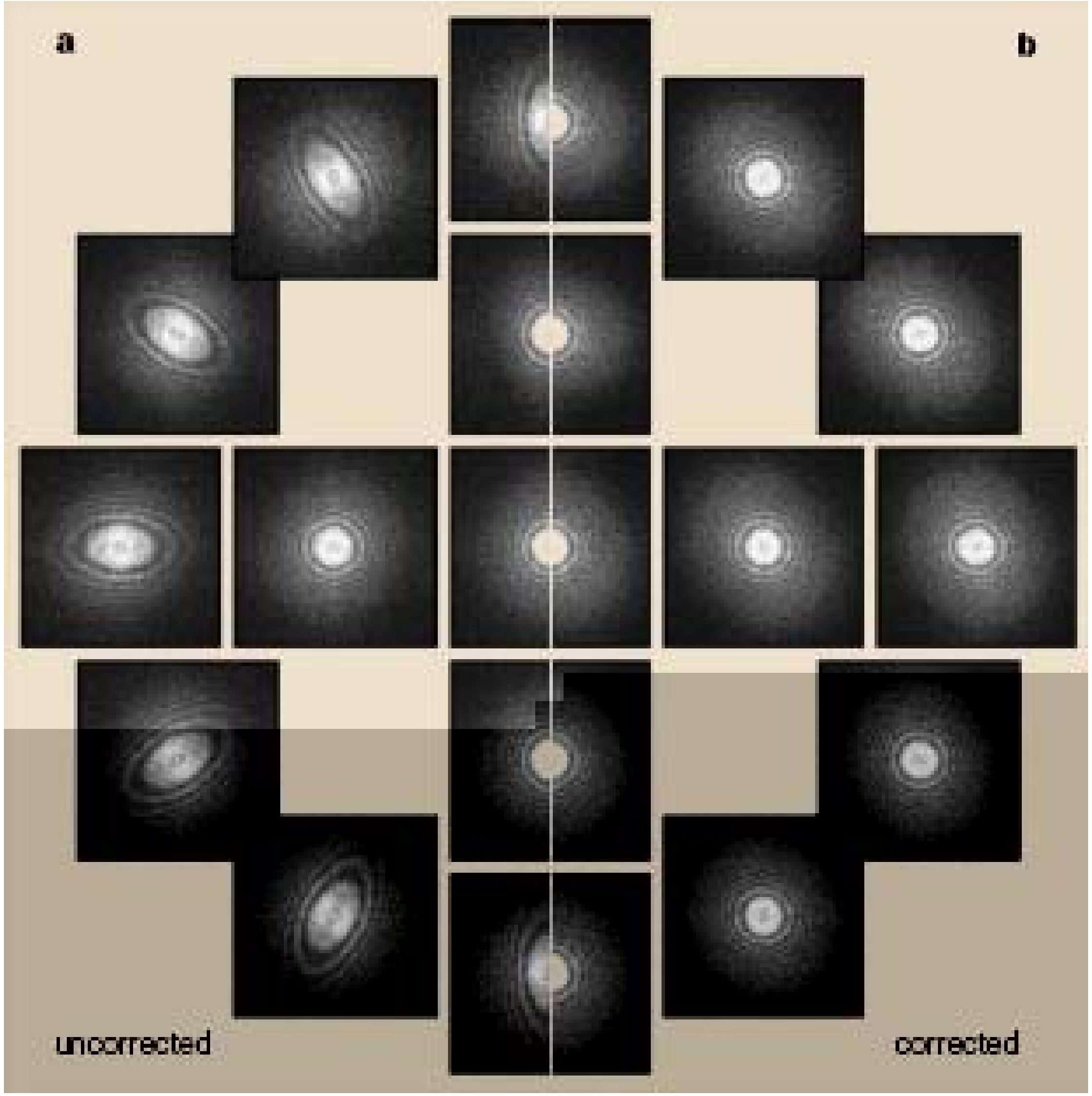

10.8A-C TEM **M.Haider, S.Uhlemann, E.Schwan, H.Rose, B.Kabius and K.Urban : Nature, 392 (1998) 768.**

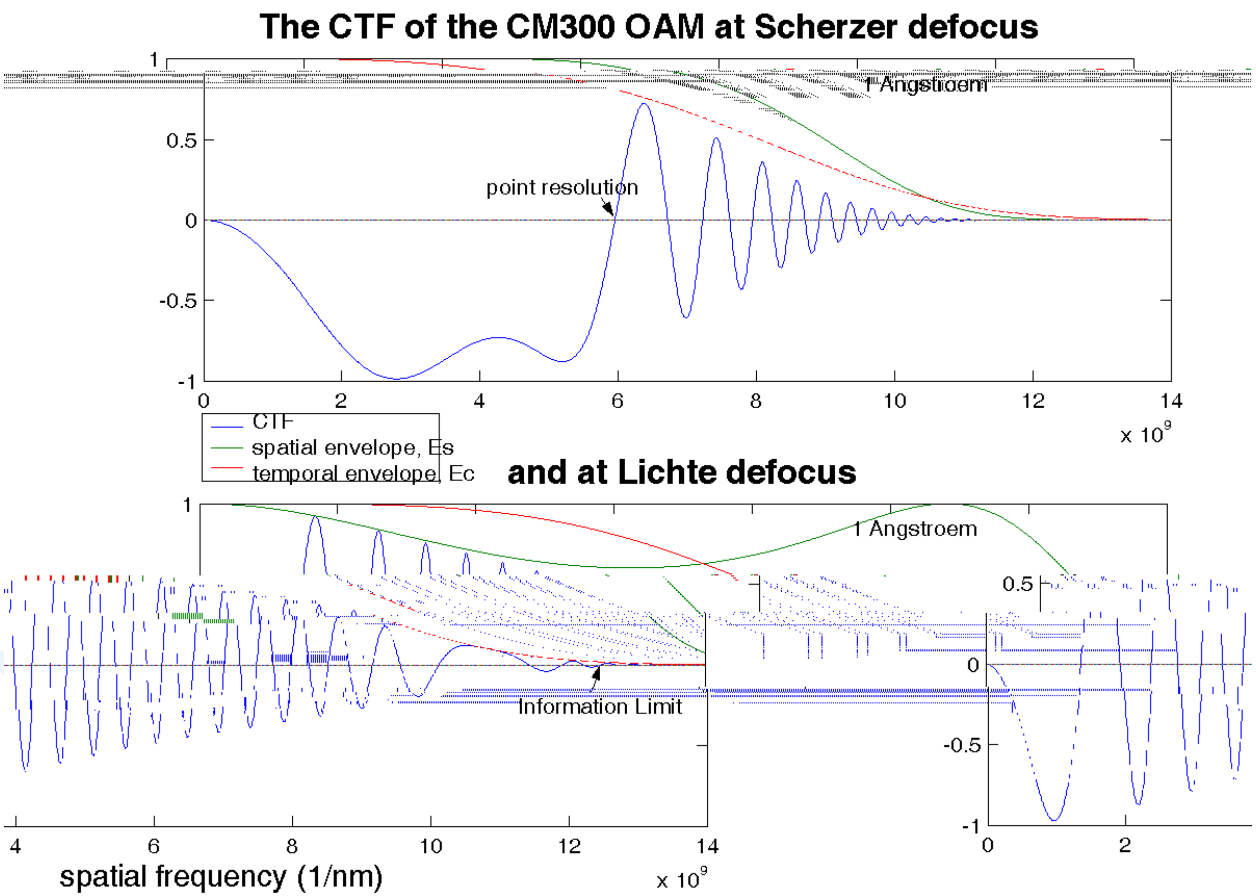
The CTF of the CM300 OAM at Scherzer defocus
1 Angstroem
point resolution
CTF
spatial envelope, Es
temporal envelope, Ec
x 10^9
and at Lichte defocus
1 Angstroem
Information Limit
spatial frequency (1/nm)
x 10^9

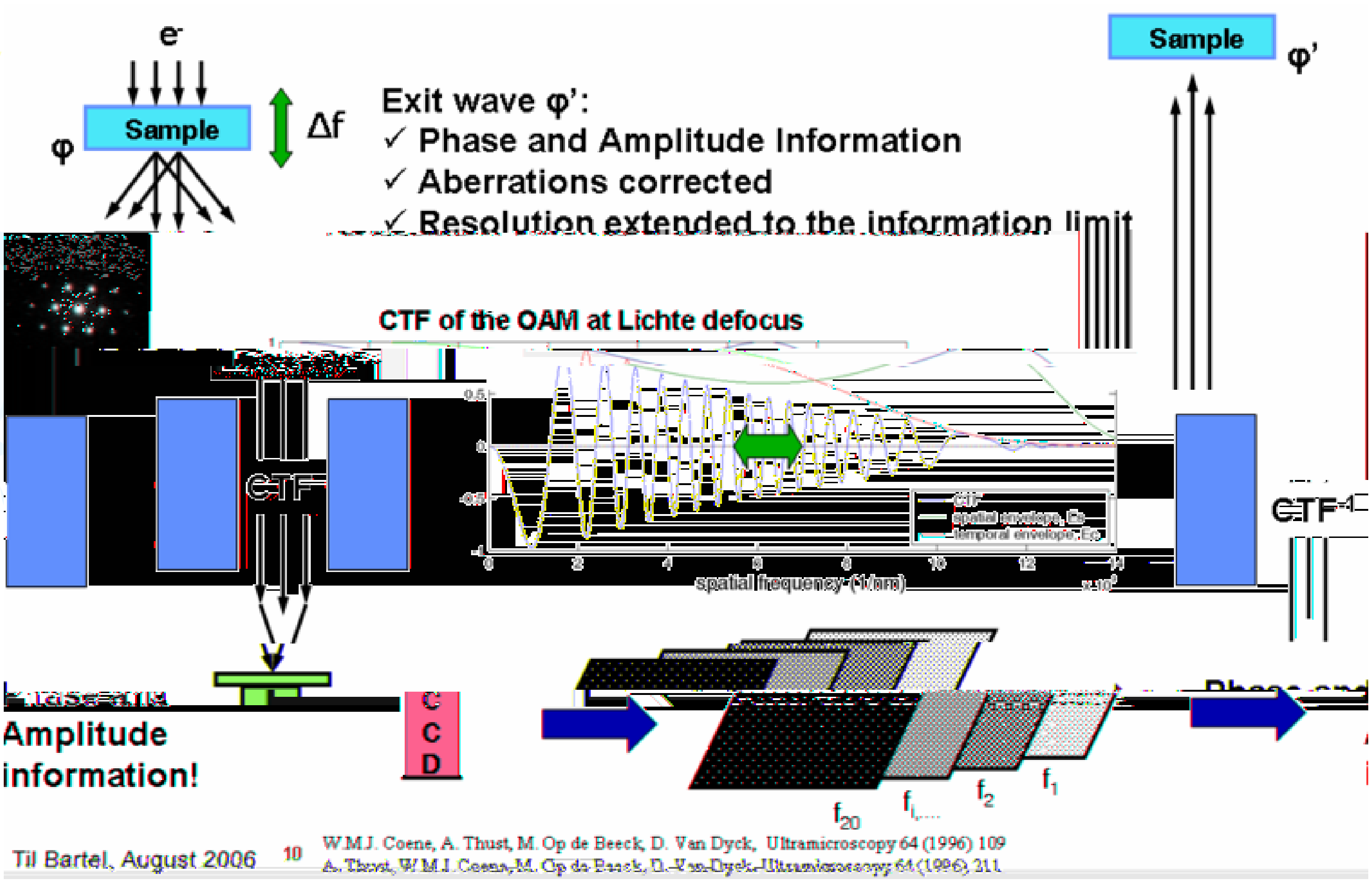

e-
Sample
φ
Δf
Exit wave φ':
✓ Phase and Amplitude Information
✓ Aberrations corrected
✓ Resolution extended to the information limit
Sample
φ'
CTF of the OAM at Lichte defocus
CTF
CTF-1
spatial frequency (1/nm)
CTF
spatial envelope, Es
temporal envelope, Et
Amplitude
information!
C
C
D
f20
fi,....
f2
f1
Til Bartel, August 2006
10
W.M.J. Coene, A. Thust, M. Op de Beeck, D. Van Dyck, Ultramicroscopy 64 (1996) 109
A. Thust, W.M.J. Coene, M. Op de Beeck, D. Van Dyck, Ultramicroscopy 64 (1996) 211

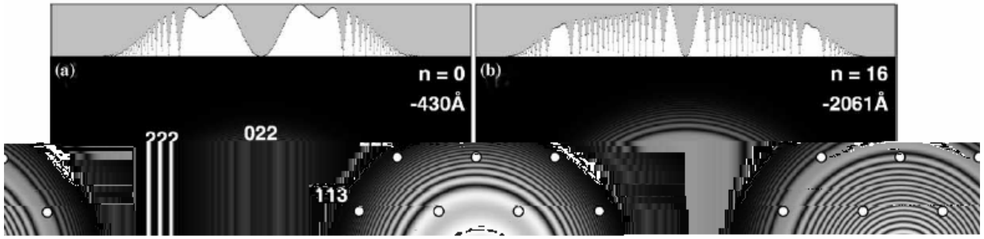

[110]

111
220
113
400

M.A. O'Keefe et al., Ultramicroscopy 89 (2001) 215–241

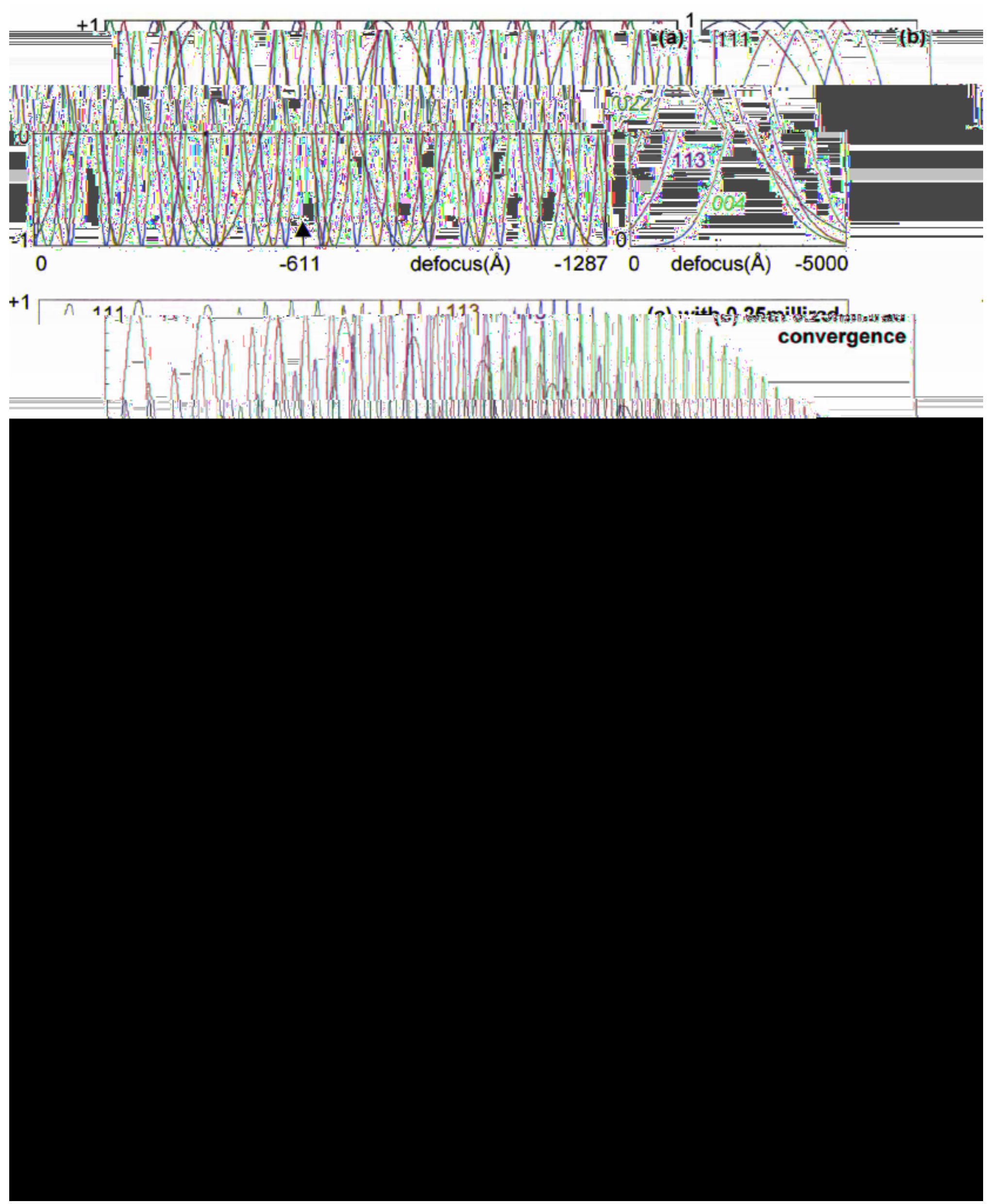

M.A. O’Keefe et al., Ultramicroscopy 89 (2001) 215–241

A_2

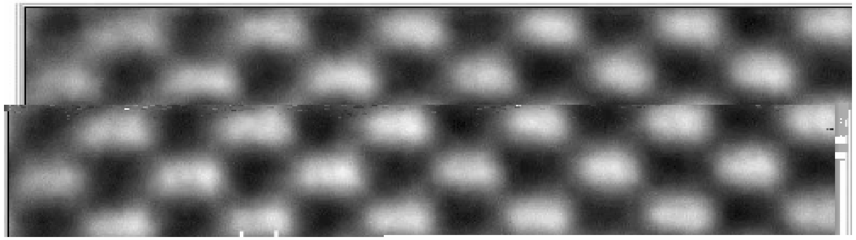

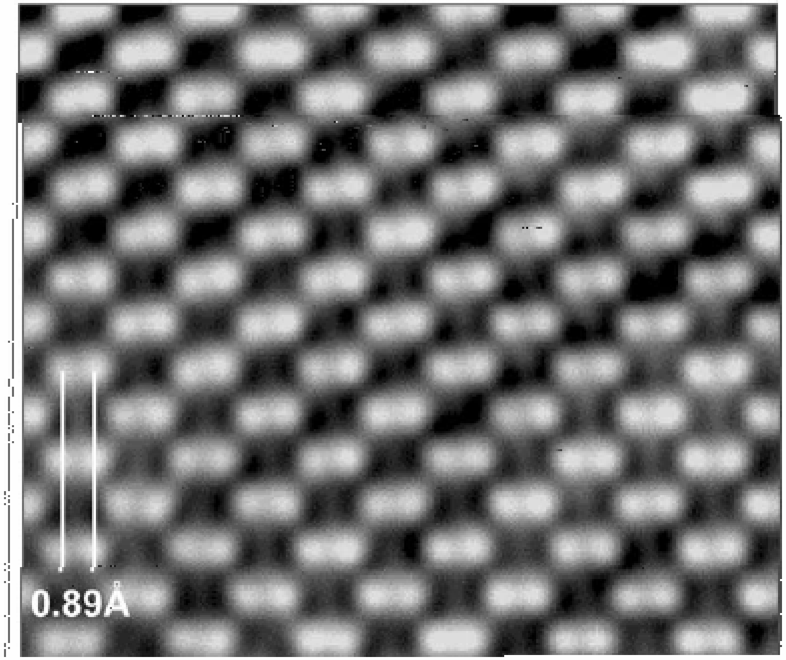

M.A. O'Keefe et al., Ultramicroscopy 89 (2001) 215–241

- $q(x,y) = \exp\{-i\sigma\phi(x,y) - \mu(x,y)\}$,

  $q(x,y) = 1 - i\sigma\phi(x,y) - \mu(x,y)$.

- $Q(u,v) = [\delta(u,v) - M(u,v) - i\sigma\Phi(u,v)]\exp\{i\chi\}$
  $= \delta(u,v) - M(u,v)\cos\chi + \sigma\Phi(u,v)\sin\chi - i\{\sigma\Phi(u,v)\cos\chi\}$

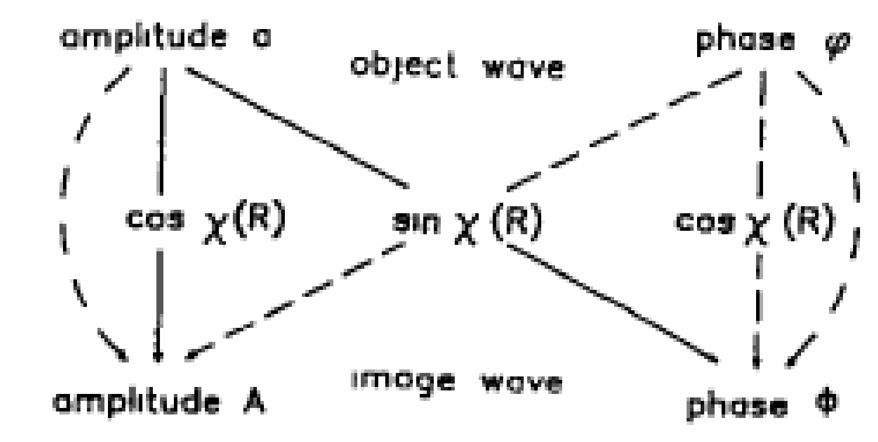

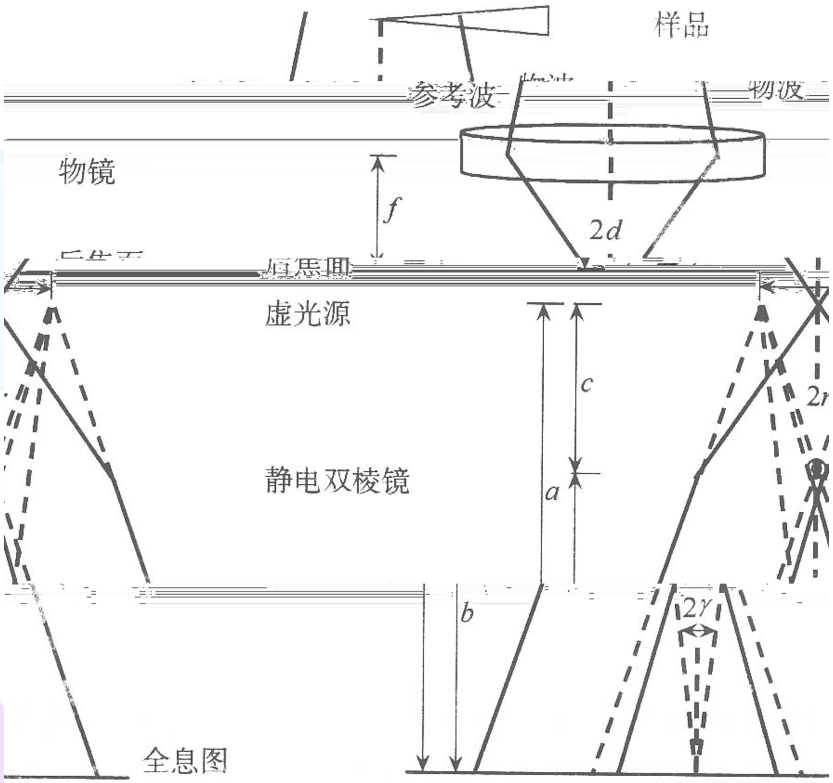
样品
参考波
物波
物镜
f
2d
虚光源
c
静电双棱镜
a
b
2γ
全息图

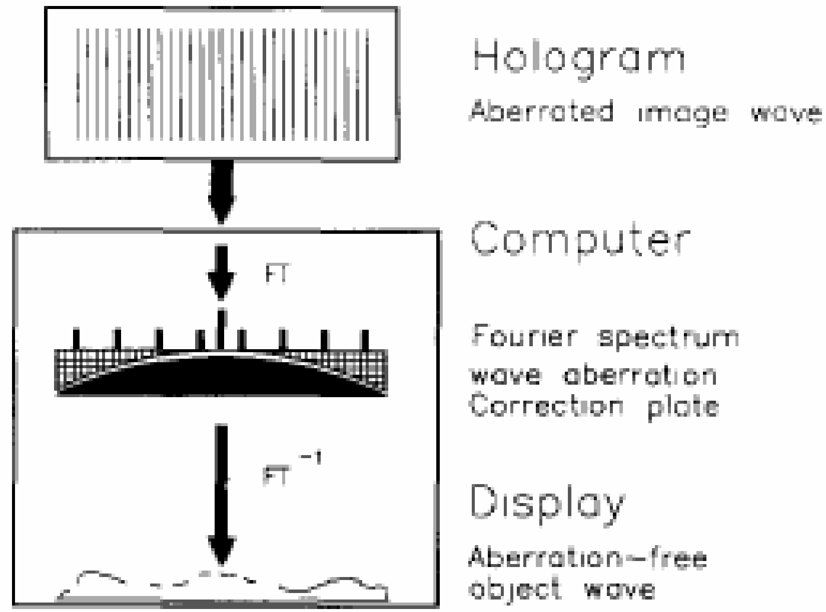
Hologram
Aberrated image wave
Computer
FT
Fourier spectrum
wave aberration
Correction plate
FT -1
Display
Aberration-free
object wave

0.0083nm

Ken Harada at al., Proceedings of 8APEM, Kazakawa, Japan, pp 90.

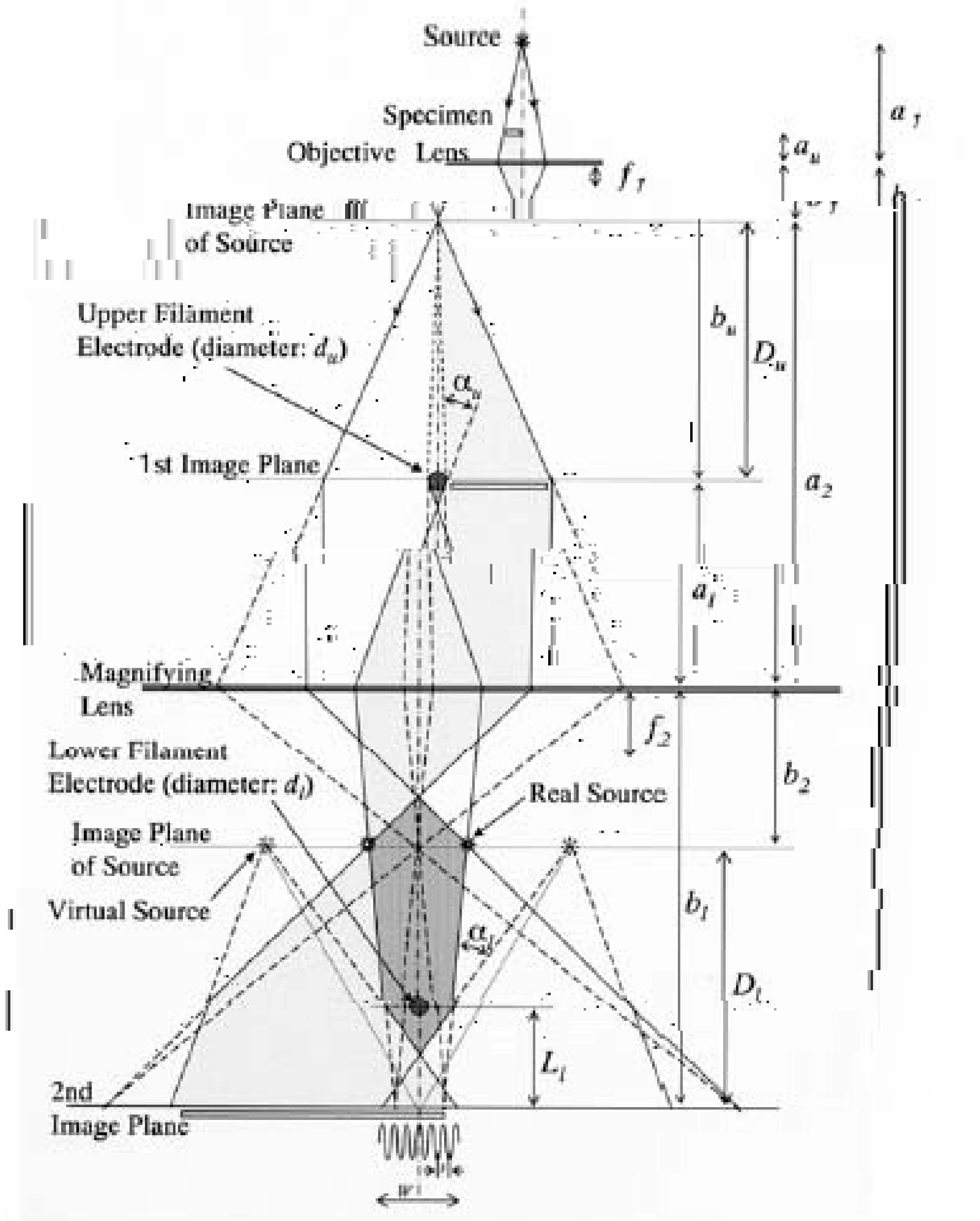

Figure 1. Optical set up of double biprism electron holography

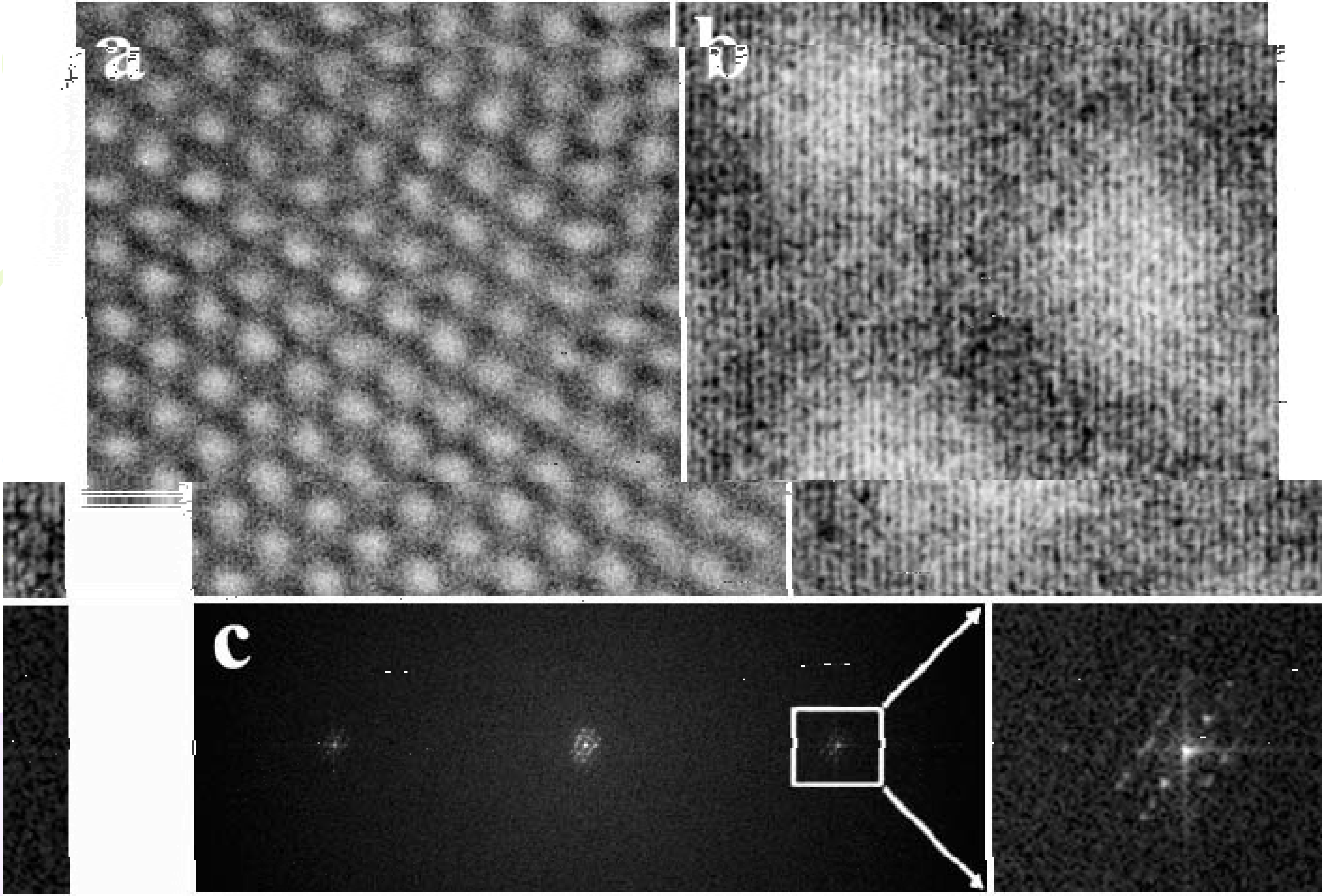

Ken Harada at al., Proceedings of 8APEM, Kazakawa, Japan, pp 100.

- Scherzer 1936 :

1948

,

,

, ,

,

O.Scherzer, (1936) Z.Phys. 101, 23;
(1948) Optik 4, 258

OX

OY

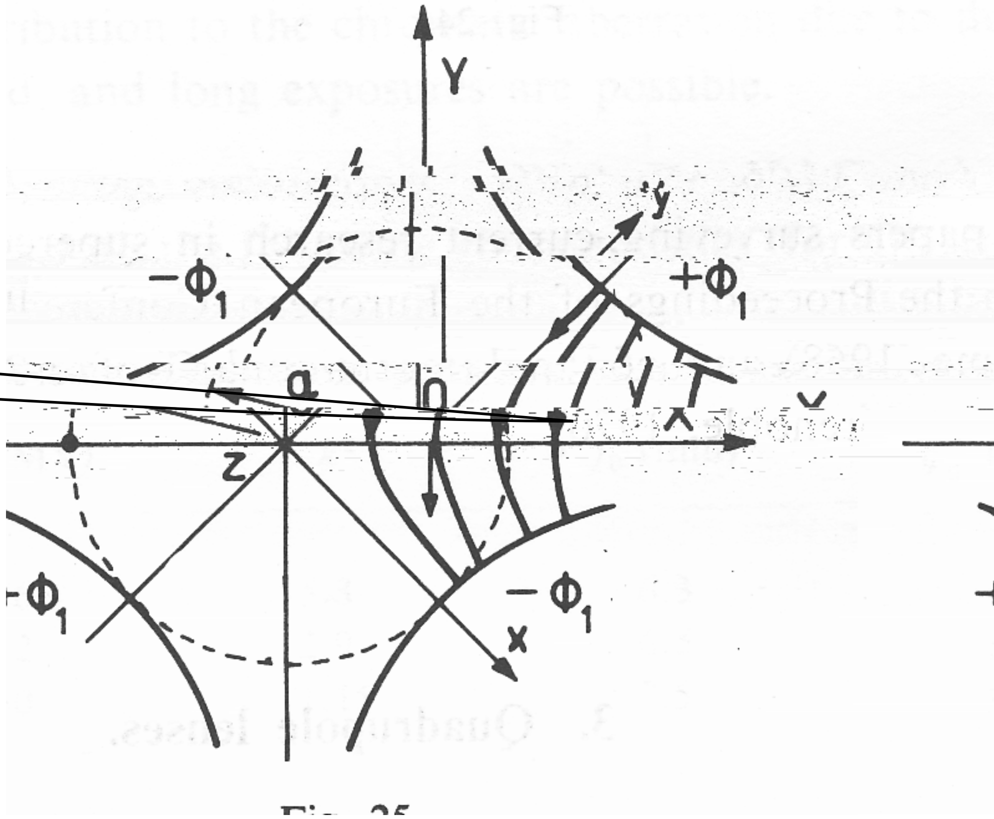

•

Q_1 C Q_2 D

k

•

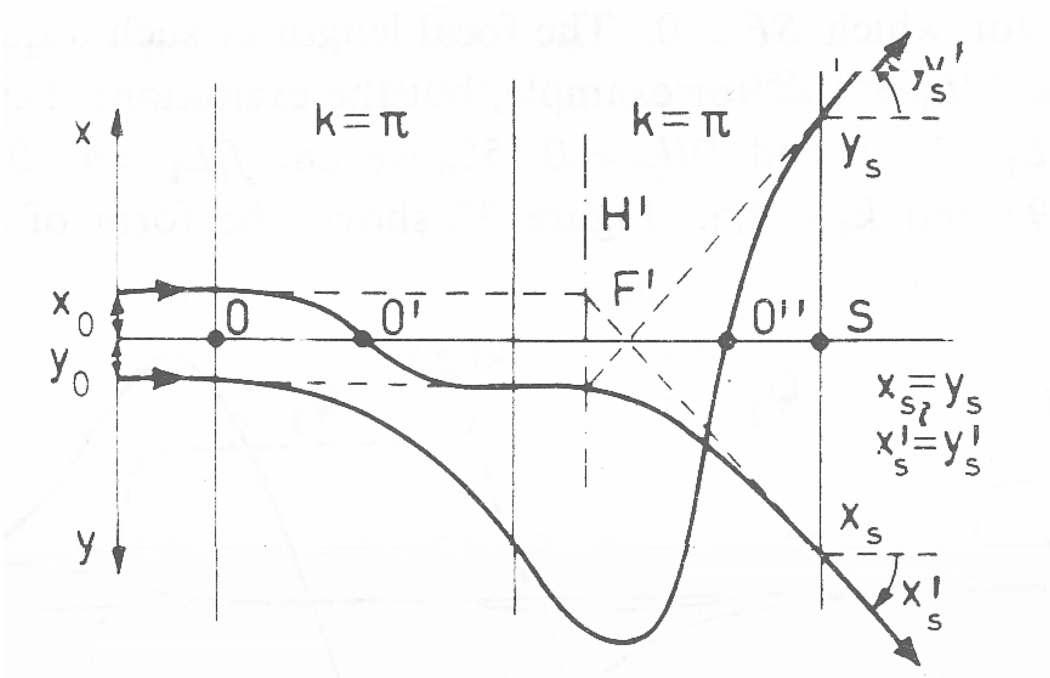

A.Septier: Chapter 2, in <<Electron Microscopy in Material Science>>, U.Valdre Edited, (1971) AP, p14-73.

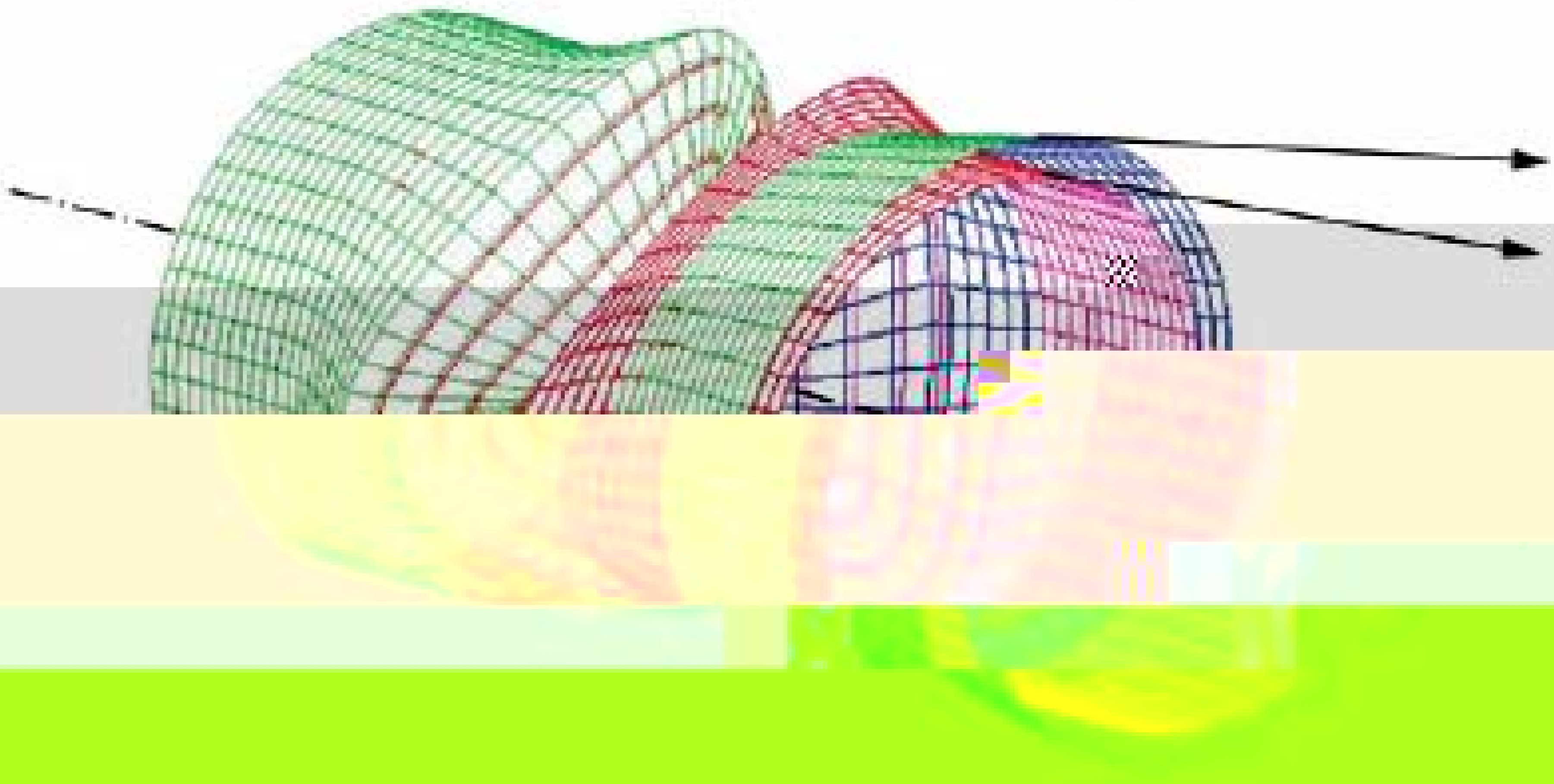

TEM,1998

Measured wave aberrations for the uncorrected microscope after the alignment

Coefficient	Measured value	Standard deviation
C_1	$-$ 590 nm	10 nm
$\|A_1\|$	0	10 nm
A_2	0.14 μm/120°	0.15 μm
B_2	0.10 μm/80°	0.15 μm
C_3	1290 μm	15 μm

Wave aberration coefficients of the corrected microscope, measured at a tilt of $|\tau| = 26$ mrad

Coefficient	Measured value	Standard deviation
C_1	$-$ 570 nm	10 nm
A_1	14 nm/146°	10 nm
A_2	250 nm/ $-$ 20°	60 nm
B_2	55 nm/ $-$ 104°	60 nm
C_3	+ 90 μm	3 μm
A_3	5.5 μm/ $-$ 59°	2 μm
S_3	1.6 μm/108°	2 μm
A_4	86 μm/154°	60 μm
B_4	30 μm/ $-$ 141°	30 μm
D_4	19 μm/ $-$ 10°	20 μm
C_5	+ 6 mm	4 mm
A_5	1 mm/150°	2 mm

S.Uhlemann & M.Haider: Ultramicroscopy 72 (1998) 119.

STEM, 2001

N.Dellby, O.L.Krivanek, P.D.Nellist, P.E.Batson, and R.Lupini: J. of EM, 50(3) (2001) 177.

Table 1 Aberration co… the Ronchigram shown… …efficients measured shortly before recording …in Fig. 3d.

Aberration coefficient	Measured value (nm)
C_1	–805.3
$C_{1,2a}$	–2.2
$C_{1,2b}$	–2.1
$C_{2,1a}$	–207
$C_{2,1b}$	–102
$C_{2,3a}$	19
$C_{2,3b}$	24
C_3	-2.6×10^4
$C_{3,2a}$	7.1×10^3
$C_{3,2b}$	1.1×10^4
$C_{3,4a}$	0.2×10^3
$C_{3,4b}$	1.8×10^4
$C_{4,1a}$	0.3×10^5
$C_{4,1b}$	2.8×10^5
$C_{4,3a}$	0.3×10^5
$C_{4,3b}$	7.1×10^5
$C_{4,5a}$	4.4×10^5
$C_{4,5b}$	-4.2×10^5
C_5	6.3×10^7
$C_{5,2a}$	5.8×10^6
$C_{5,2b}$	-3.0×10^6
$C_{5,4a}$	-9.8×10^6
$C_{5,4b}$	-3.9×10^7
$C_{5,6a}$	-4.8×10^6
$C_{5,6b}$	1.4×10^6

π/4

2008

List of the upper limits with respect to the π/4 criterion of all axial aberrations considering only one particular aberration coefficient

Aberration	80 kV	120 kV	200 kV		300 kV
	80 pm	65 pm	100 pm	50 pm	50 pm
Focus C_1 (nm)	0.40	0.31	1.0	0.25	0.4
Two-fold astigmatism A_1 (nm)	0.40	0.31	1.0	0.25	0.4
Three-fold astigmatism A_2 (nm)	11.50	9.2	60.0	7.5	13
Second-order coma B_2 (nm)	3.80	3.1	20.0	2.5	5.0
Third-order spherical aberr. C_3 (μm)	0.30	0.24	3.2	0.2	0.5
Four-fold astigmatism A_3 (μm)	0.30	0.24	3.2	0.2	0.5
Third-order star aberr. S_3 (μm)	0.07	0.06	0.8	0.05	0.11
Five-fold astigmatism A_4 (μm)	8.2	6.4	16.0	5.0	13.
Fourth-order coma B_4 (μm)	1.65	1.3	3.2	1.0	2.6
Fourth-order three-lobe aberr. D_4 (μm)	1.65	1.3	3.2	1.0	2.6
Fifth-order spher. aberr. C_5 (mm)	0.17	0.13	7.68	0.12	0.4
Six-fold astigmatism A_5 (mm)	0.17	0.13	7.68	0.12	0.4
Fifth-order rosette aberr. R_5 (mm)	0.03	0.02	1.28	0.02	0.06
Fifth-order star aberr. S_5 (mm)	0.03	0.02	1.28	0.02	0.06
Seven-fold astigmatism A_6 (mm)	4.58	3.62	358.4	2.8	11.7
Sixth-order coma B_6 (mm)	0.65	0.52	51.2	0.4	1.7
Sixth-order three-lobe aberr. D_6 (mm)	0.65	0.52	51.2	0.4	1.7
Sixth-order pentacle aberr. F_6 (mm)	0.65	0.52	51.2	0.4	1.7
Seventh-order spher. aberr. C_7 (mm)	104	82.0	15904	62.2	339
Chromatic aberr. C_{c1} (μm)	10.	10.	10.	10.	10.

The summation of the total phase shift when all aberrations are contributing to the upper limit is not included.

M. Haider, H. Muller, S. Uhlemann, J. Zach, U. Loebau, R. Hoeschen:Ultramicroscopy 108 (2008) 167–178

- xoz

yoz

- SEM
- TEM

Hieder

2008-10-15

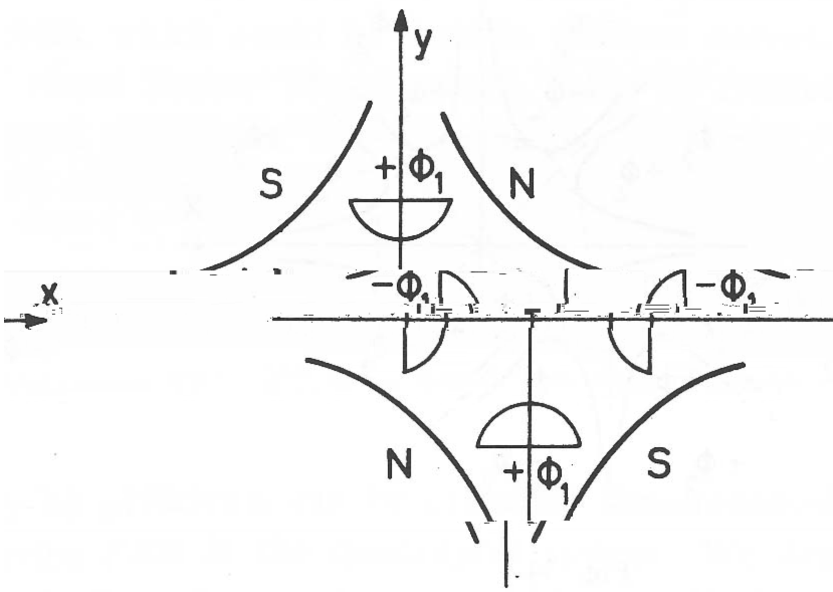

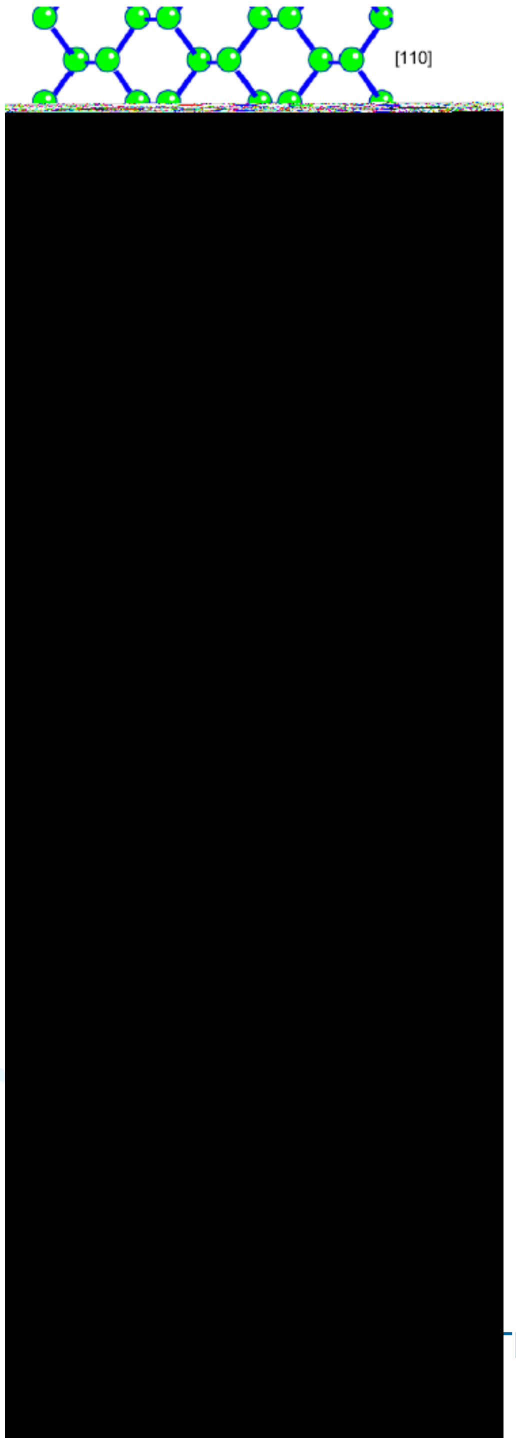

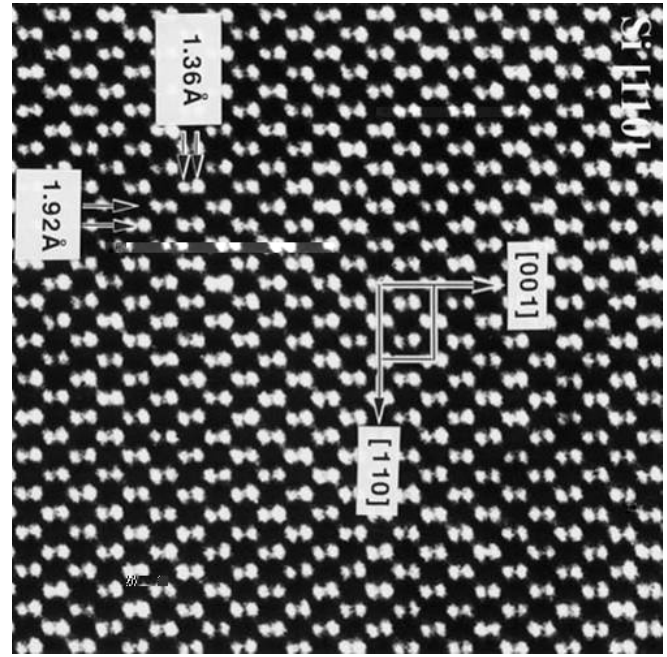

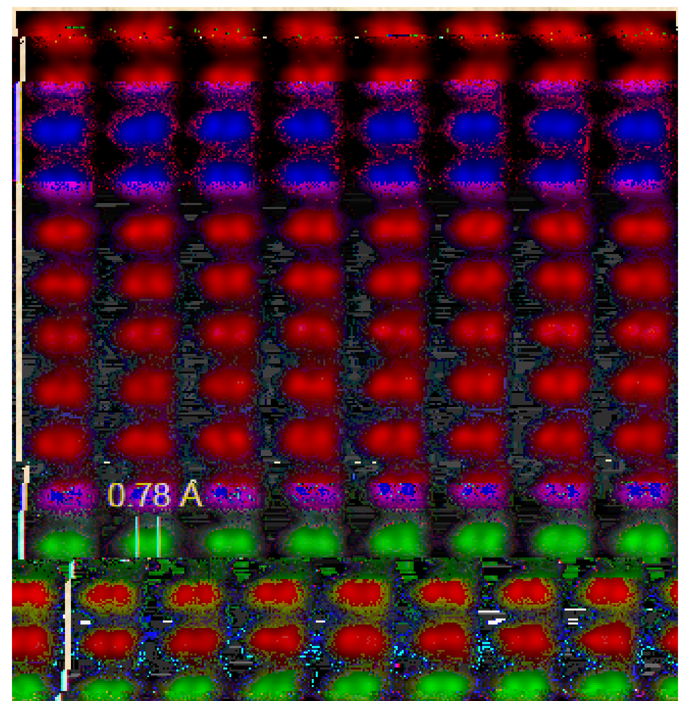

P.D. Nellist et al., Science 305, (2004)1741.

0.5

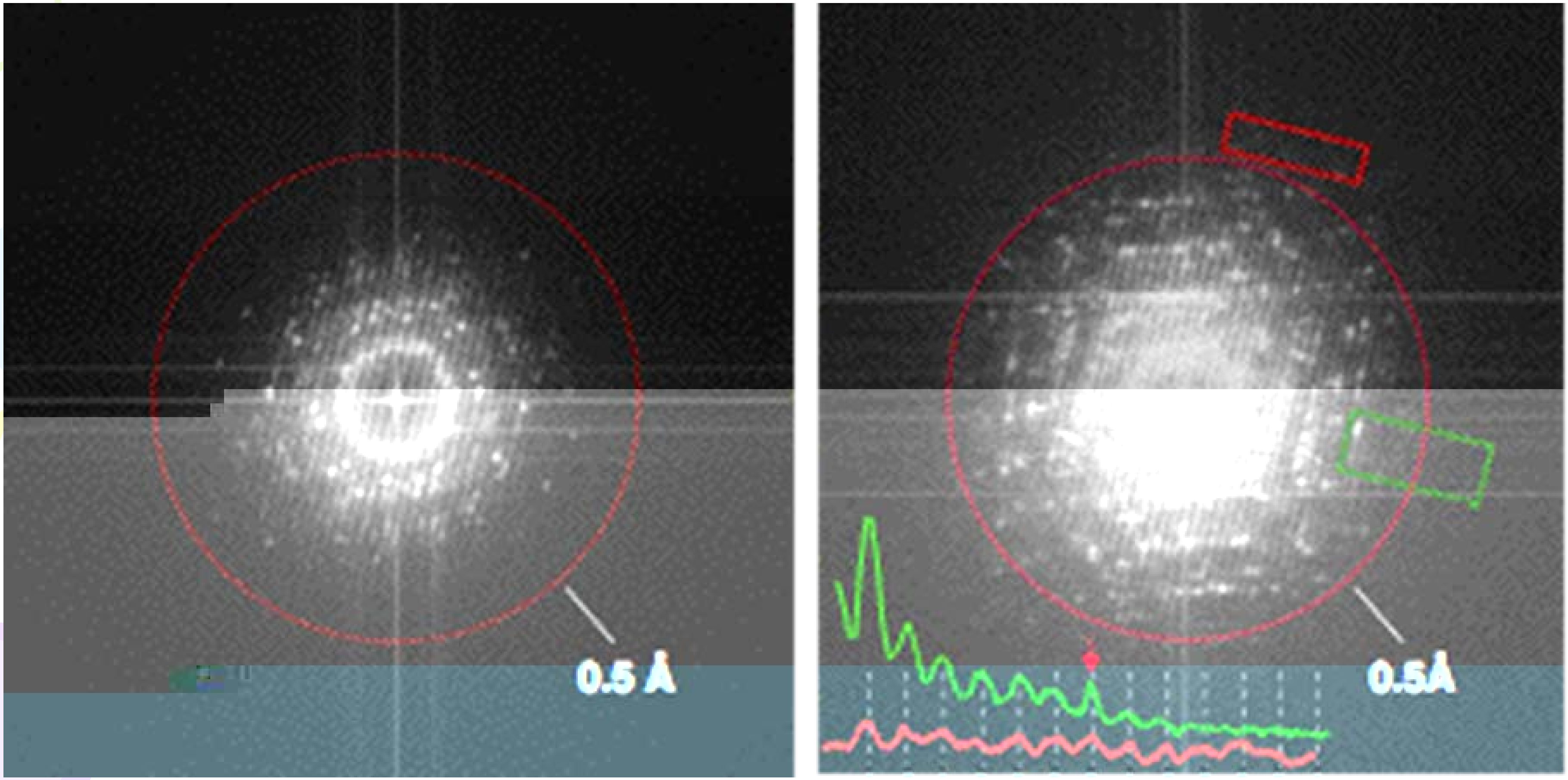

TEAM 2008

- 1
Scherzer
0.5
Si
1.11 Å,
116
0.31 Å
Debye-
Waller
0.4668 Å², 1.11 Å
0.31 Å
12

(M.A.O'Keefe:
Ultramicroscopy 108 (2008)

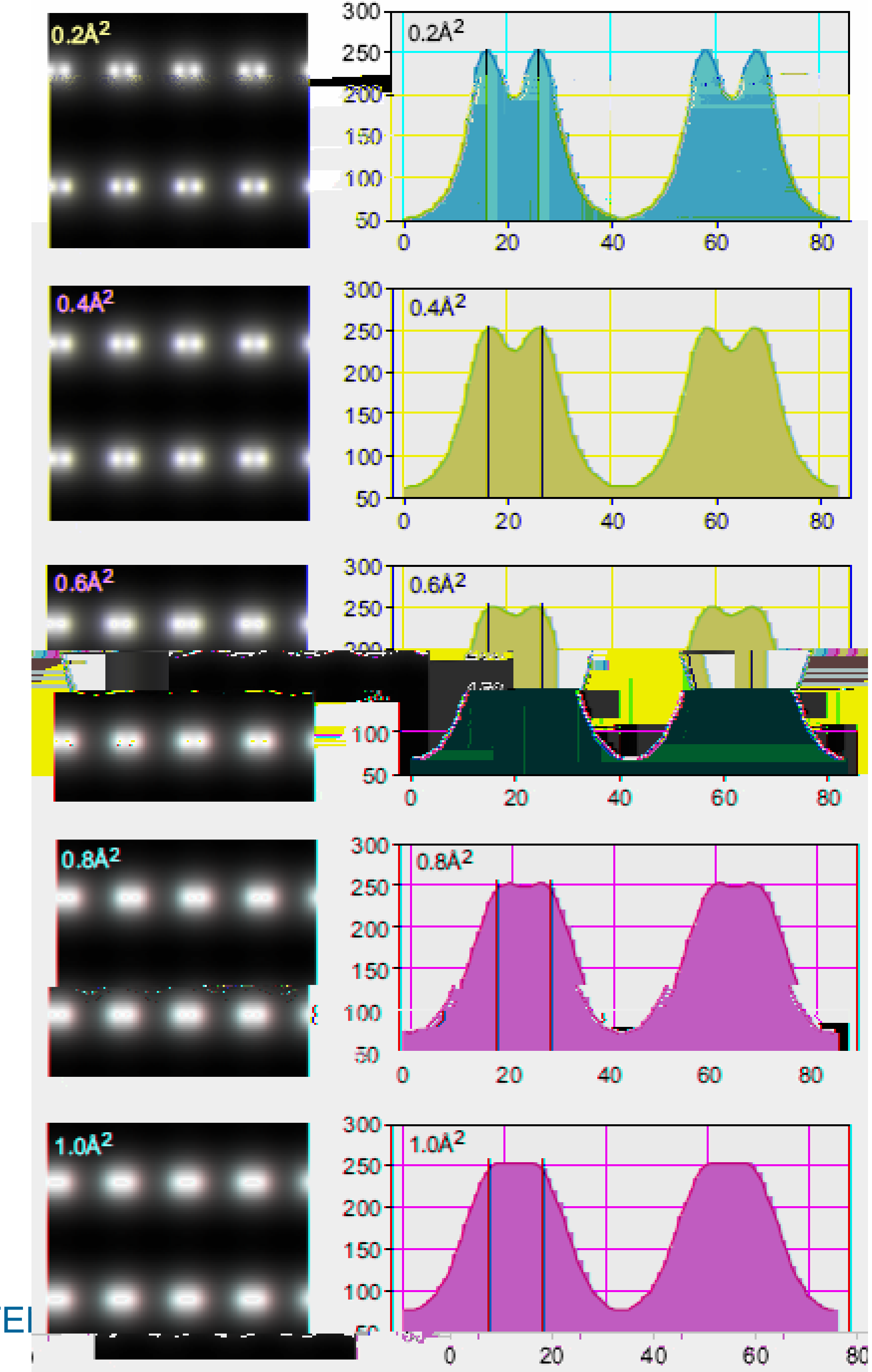

$$I = qq * \frac{1 - \sigma\lambda H \Delta f \nabla^2 \phi_p(x)}{2\pi}$$

•

f=0

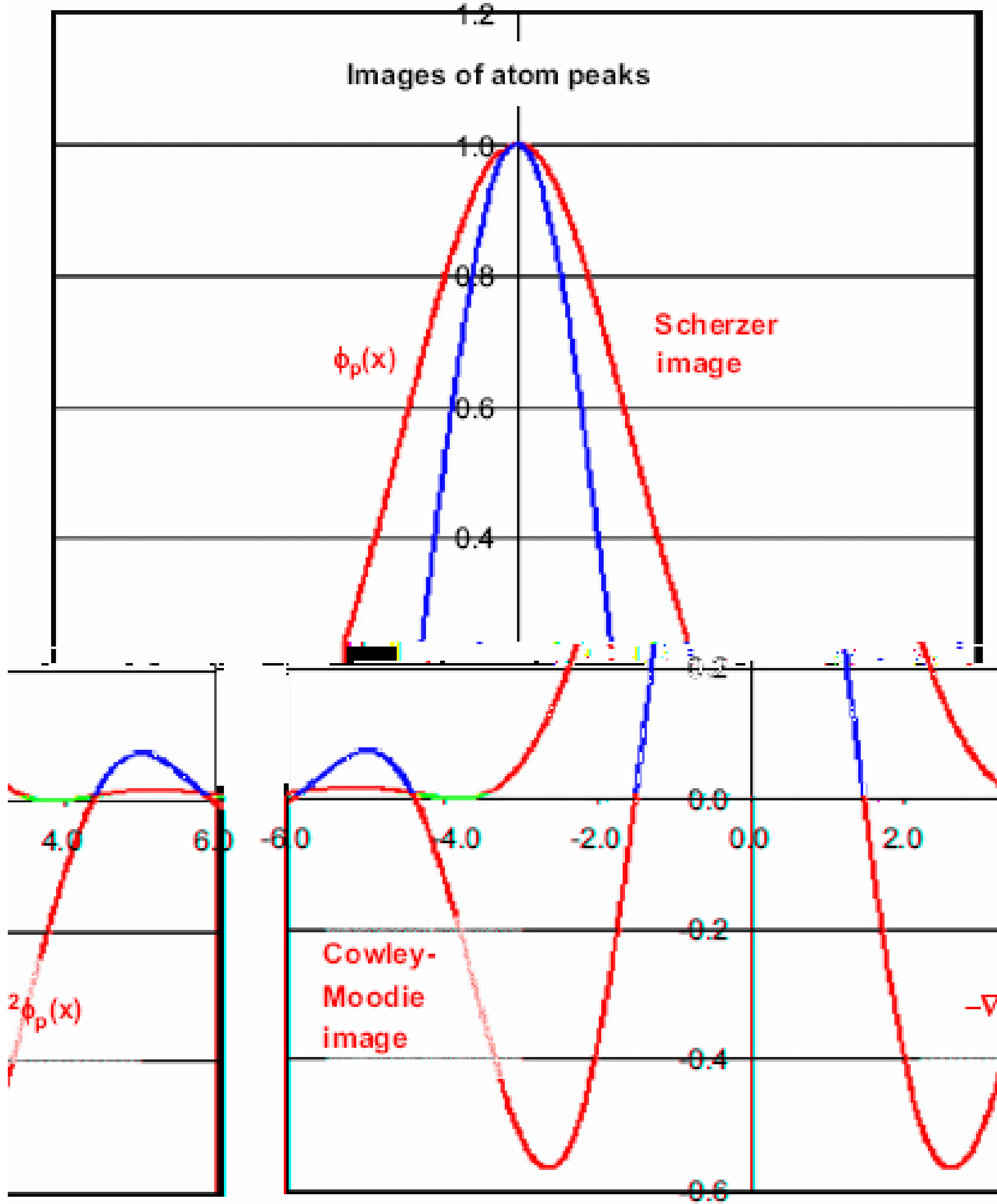

[M.A.O'Keefe: Ultramicroscopy 108 (2008) 196] "

" "

" " "

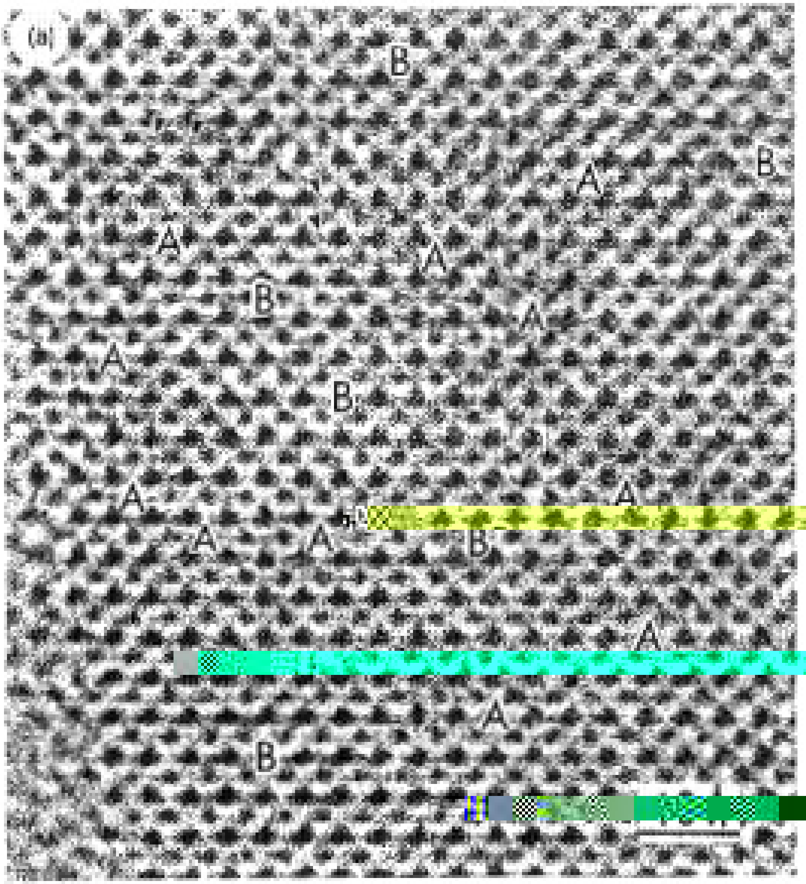

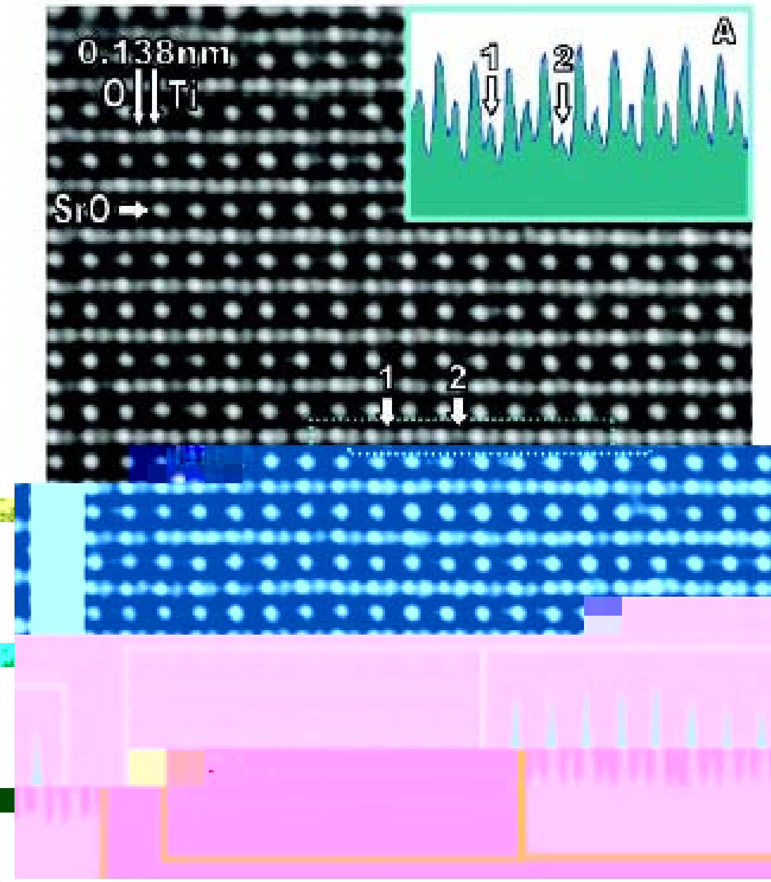

1994 1.1

1500 [S. Horiuchi, Y.Mastui and B.Okai: Jpn. J. Appl. Phys. 31 (1992) L59]

ScTiO3( )

[C.L.Jia et al., Science 299 (2003) 870]

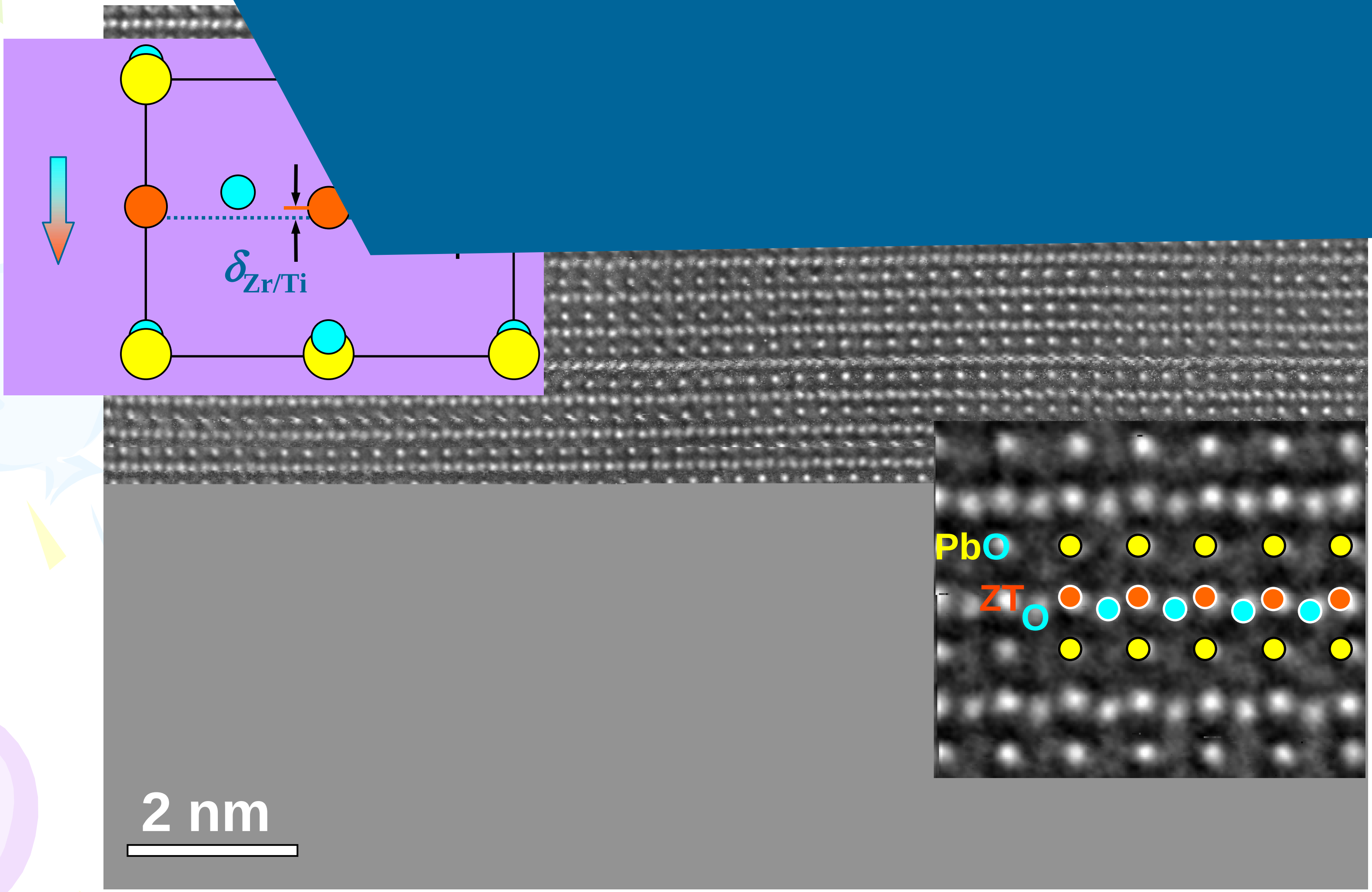

$\delta_{Zr/Ti}$
PbO
ZT
O
2 nm

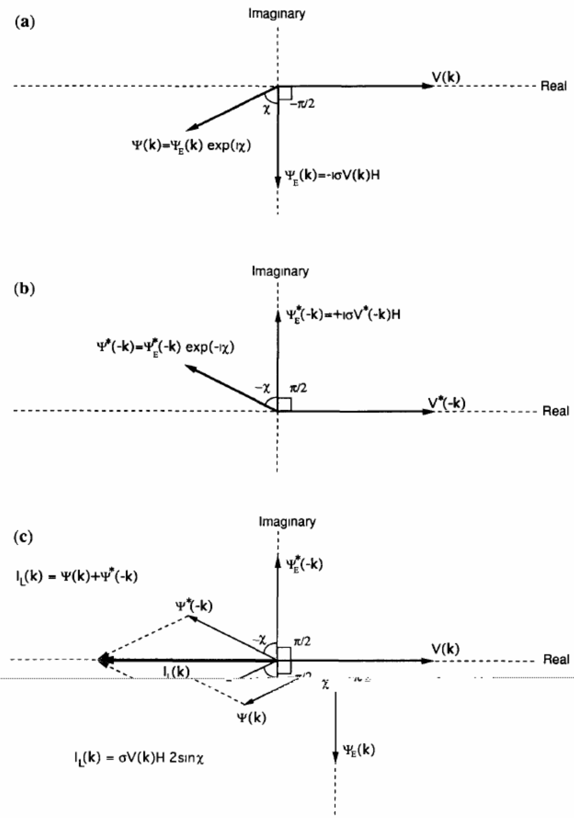

Fig 2 Argand diagrams showing the action of sin $\chi(k)$ under WPO conditions (a) Formation of the kth image a[…] component $\Psi(k)$ The specimen potential component $V(k)$ gives rise to an exit-surface diffracted beam $\Psi_E(k)$ at difference of $-\pi/2$ from $V(k)$ Passage through the objective lens rotates the phase of $\Psi_E(k)$ through an angle of $\chi(k)$ $\Psi(k)$ (b) Formation of the second amplitude component contributing to the kth image intensity component (c) Summati[…] two amplitude components to produce the intensity component $I_L(k)$, which lies along the negative extension of the origi[…] and has an amplitude (length) proportional to 2 sin $\chi(k)$

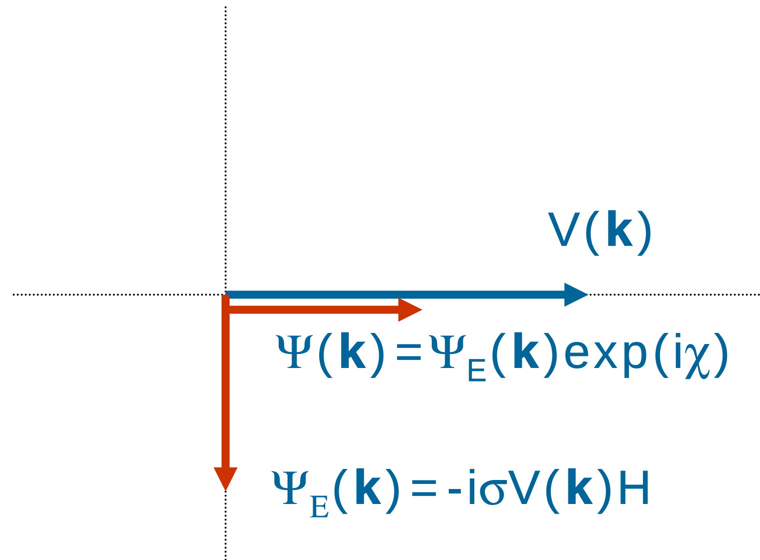

M.O'Keefe: UltraM, 47(1992) 282

+/-6pm

$YBa_2Cu_3O_{7-\delta}$

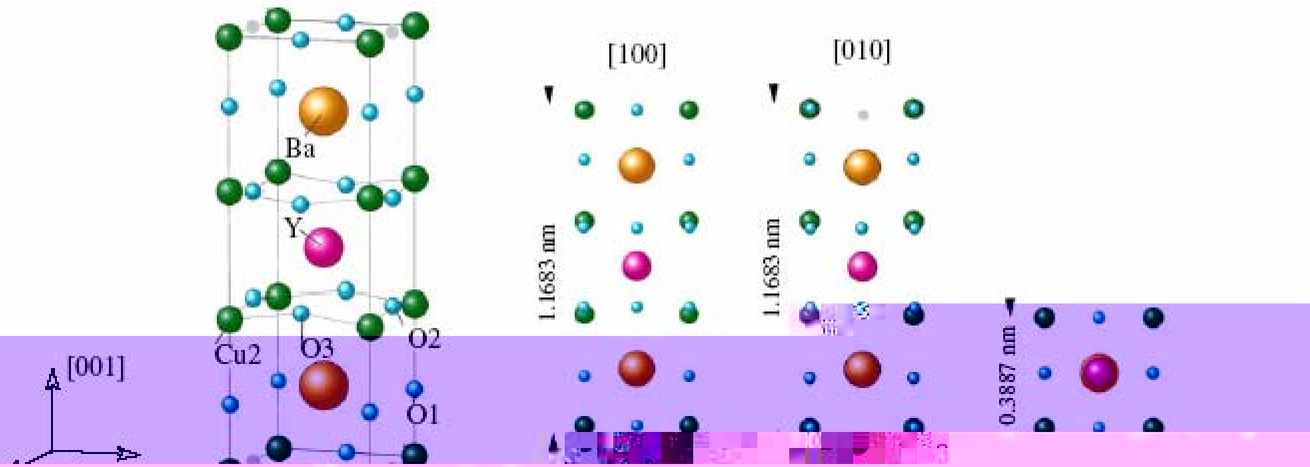

90°

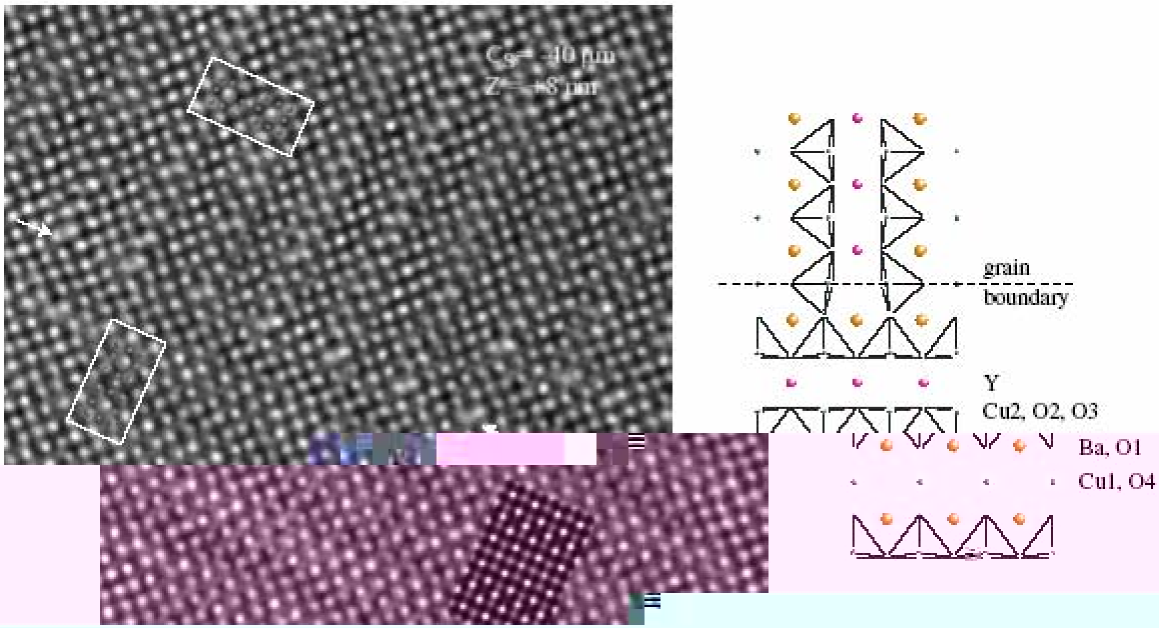

L. Houben, A. Thust, K. Urban: Ultramicroscopy 106 (2006) 200–214

20

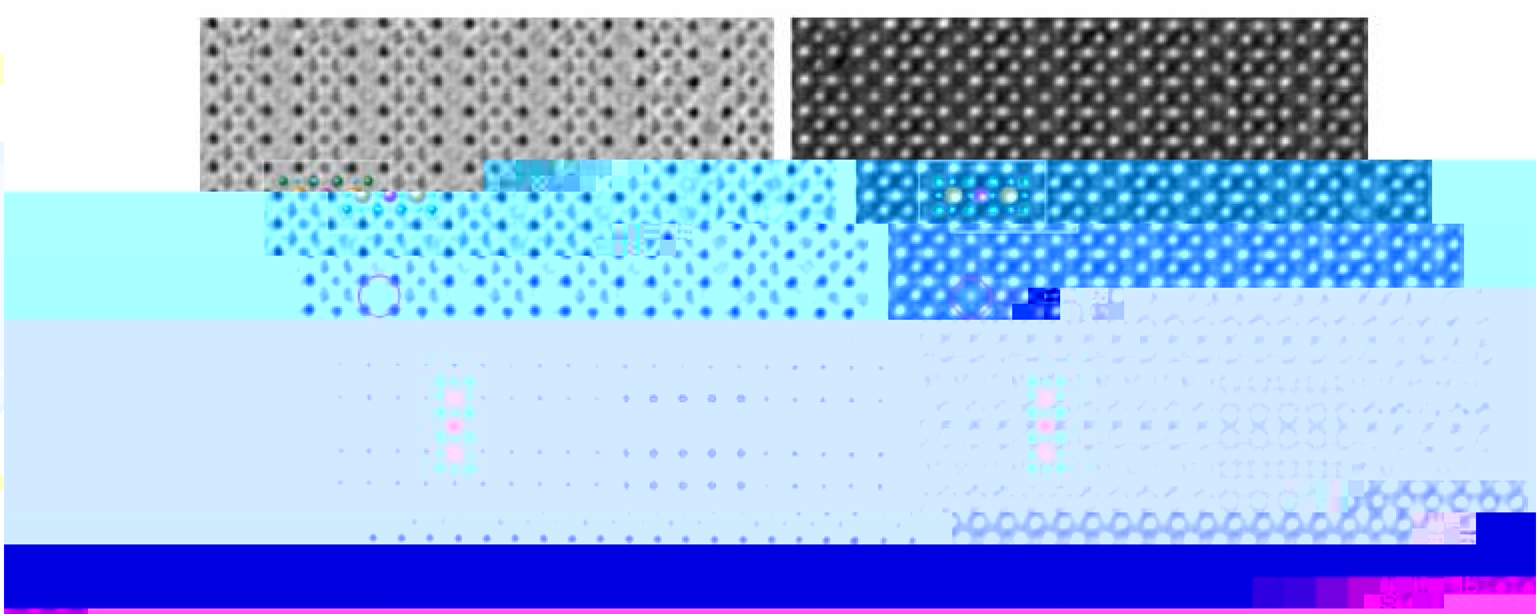

to the boundary over in the boxed regions. contrast in the grain

Fig. 6. Magnified region of the exit-plane wave function showing the grain boundary structure averaged parallel five repeat cells. (a) Amplitude image and (b) phase image. Unit cell projections along the [1 0 0] axis are shown The insets at the lower right display simulated exit-plane wave data. The circle highlights a Cu1 site of deviating boundary plane.

L. Houben, A. Thust, K. Urban: Ultramicroscopy 106 (2006) 200–214

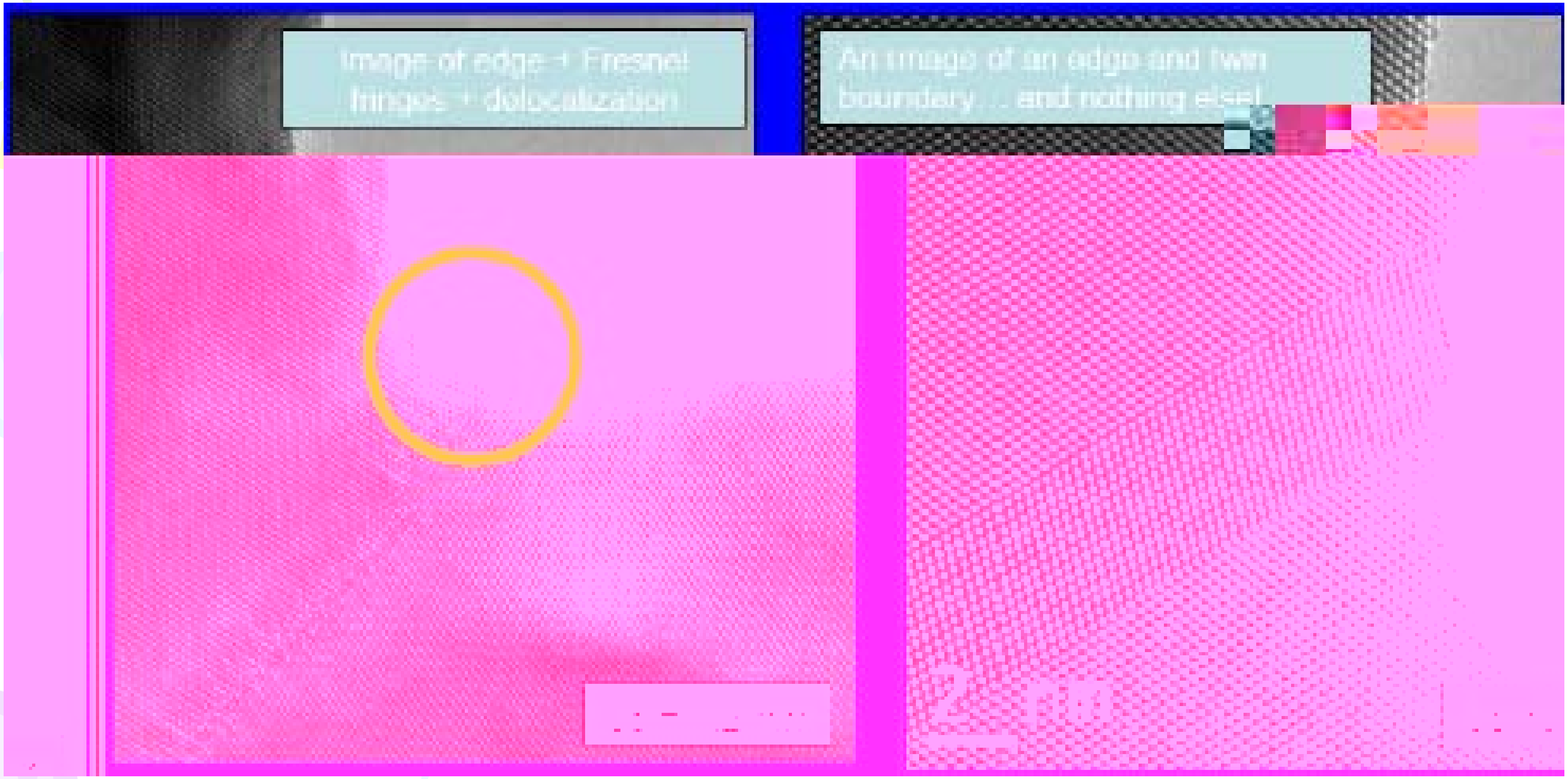

B. Freitag, S.Kujawa, P.M.Mul, J.Ringnalda, P.C.Tiemeijer: Ultramicroscopy 102 (2005) 209.

-- STEM

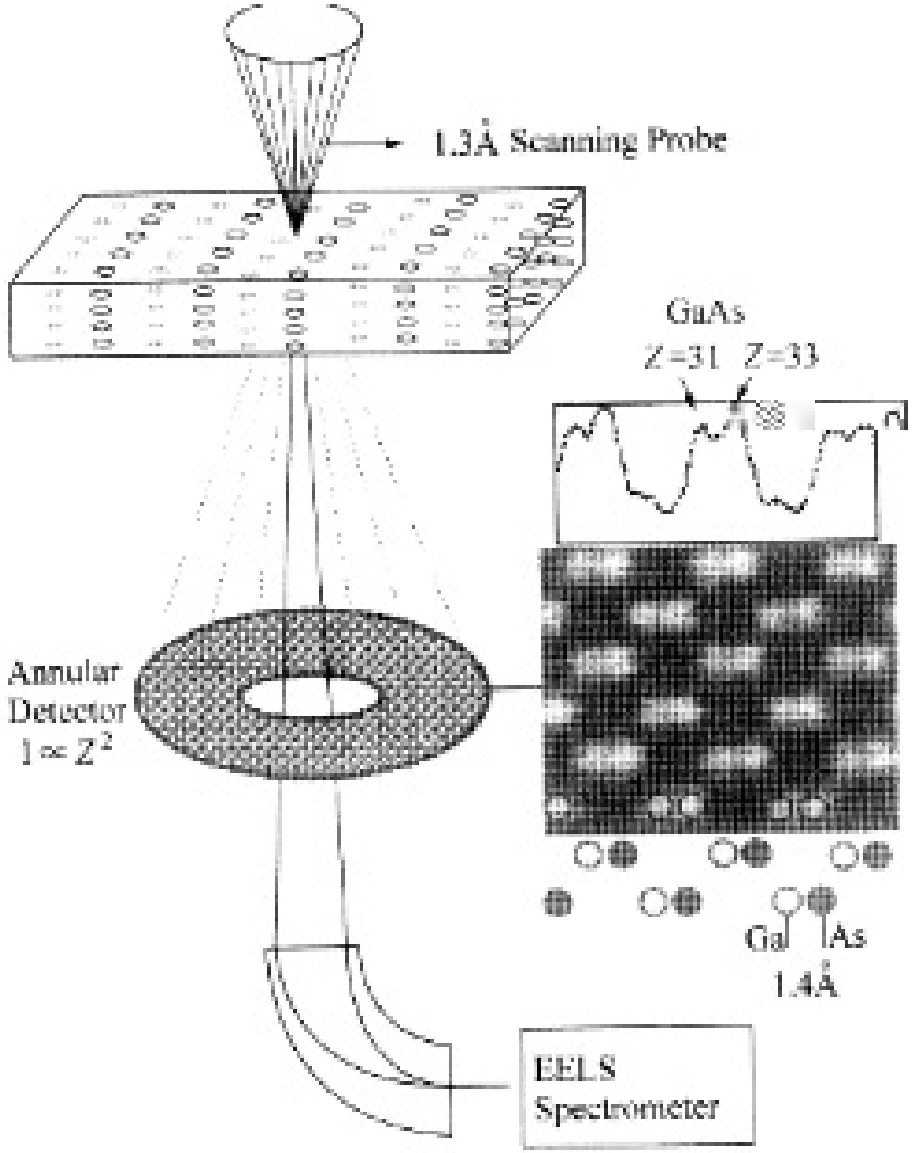
1.3Å Scanning Probe
GaAs
Z=31 Z=33
Annular
Detector
I ∝ Z²
Ga
As
1.4Å
EELS
Spectrometer

Increasing beam current

- For 0.1-0.2 nm beam size, beam current increases 1-2 order.
- It is benefit to EELS analysis with atomic resolution.
- Improve electron lithography.
- Easier radiation damage.

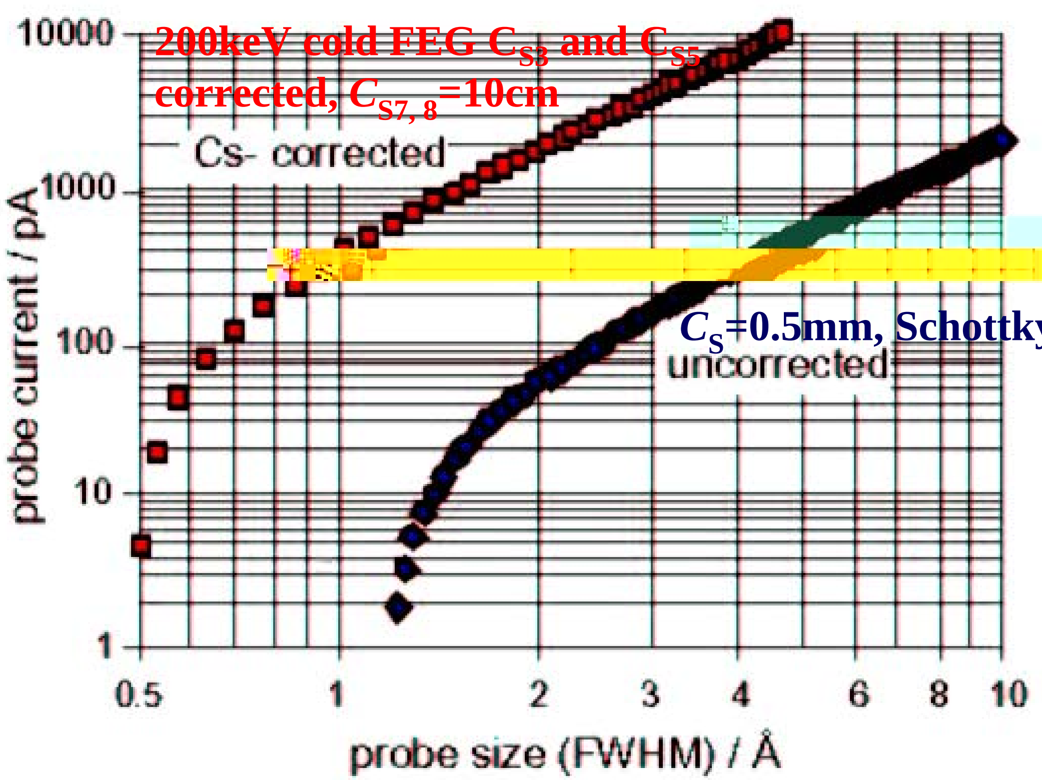

- 1
1nm
Nion
STEM 4~6 STEM
10 mrad
4
16
Schottky 10
0.78 nA

- $La_{0.7}Sr_{0.3}MnO_3$ / $SrTiO_3$

3.1nm

A La M

La

C Mn L

Mn

La

La Mn

1.9 Å B Ti

L D

Mn La Ti

[D.A.Muller, L.F.Kourkoutis, M.Murfitt, J.H.Song, H.Y.Hwang, J.Silcox, N.Dellby, and O.L.Krivanek: Science 319 (2008) 1073]

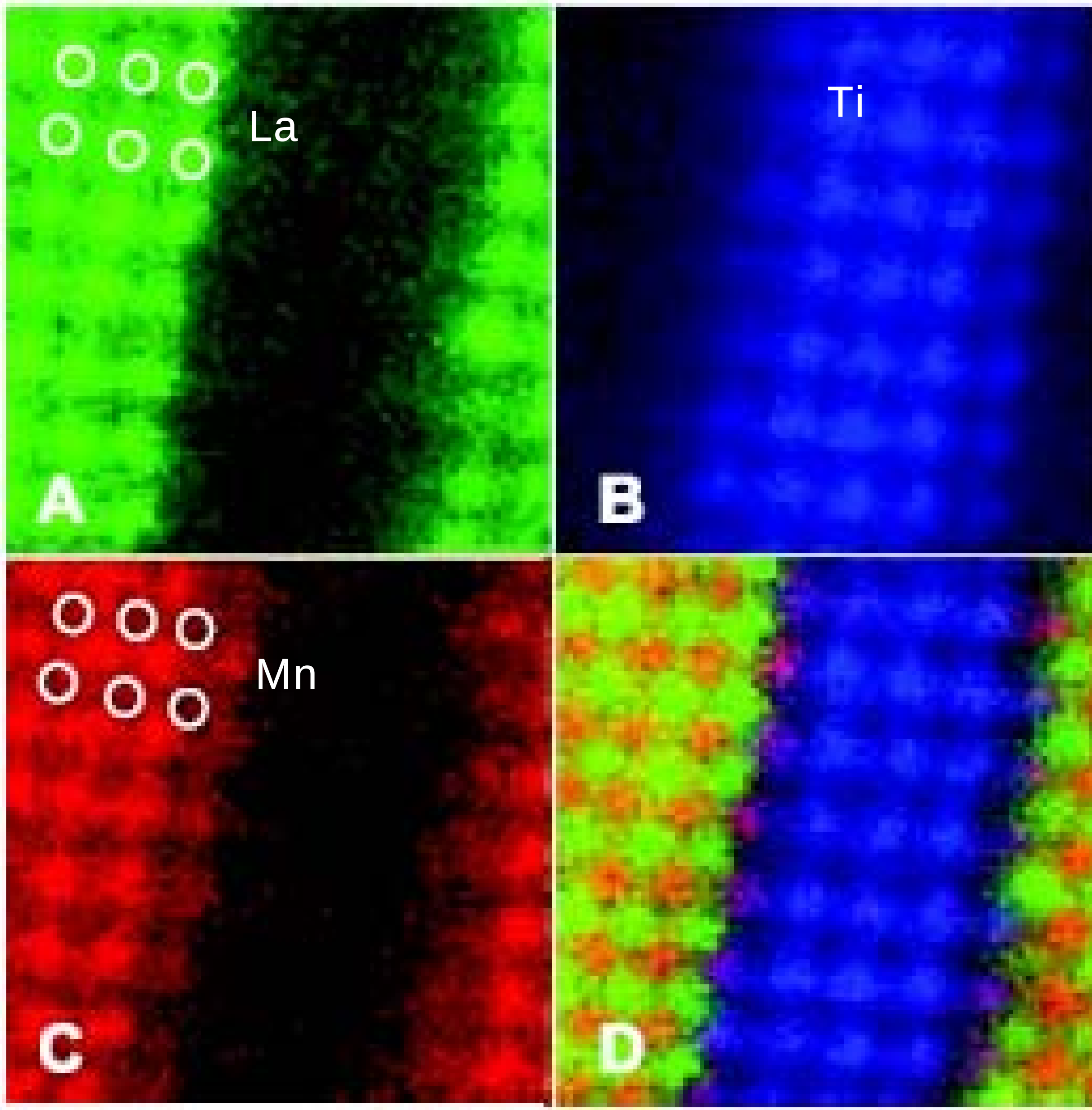

- Ni
Nb Zr
XEDX (c)
Nb

(d) Zr
(e)
Zr
f
Zr

[M. Watanabe, D.W. Ackland, A. Burrows, C.J. Kiely, D.B. Williams, O.L. Krivanek, N. Dellby, M.F. Murfitt, and Z. Szilagyi: Microsc Microanal. 12, (2006) 515]

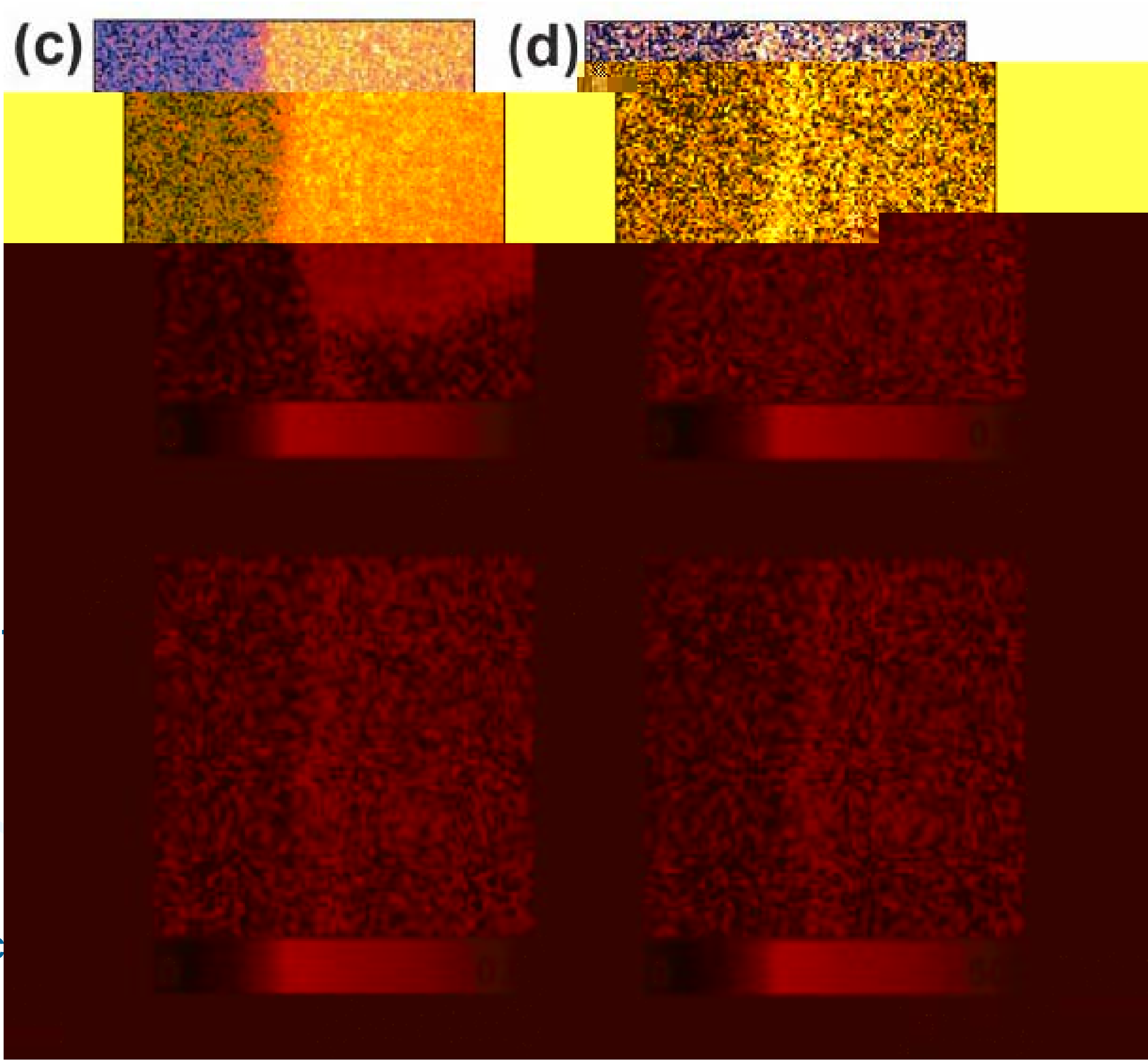

STEM

AC-STEM

- 35mrad.
  300 STEM
  1 nm
  50mrad 5

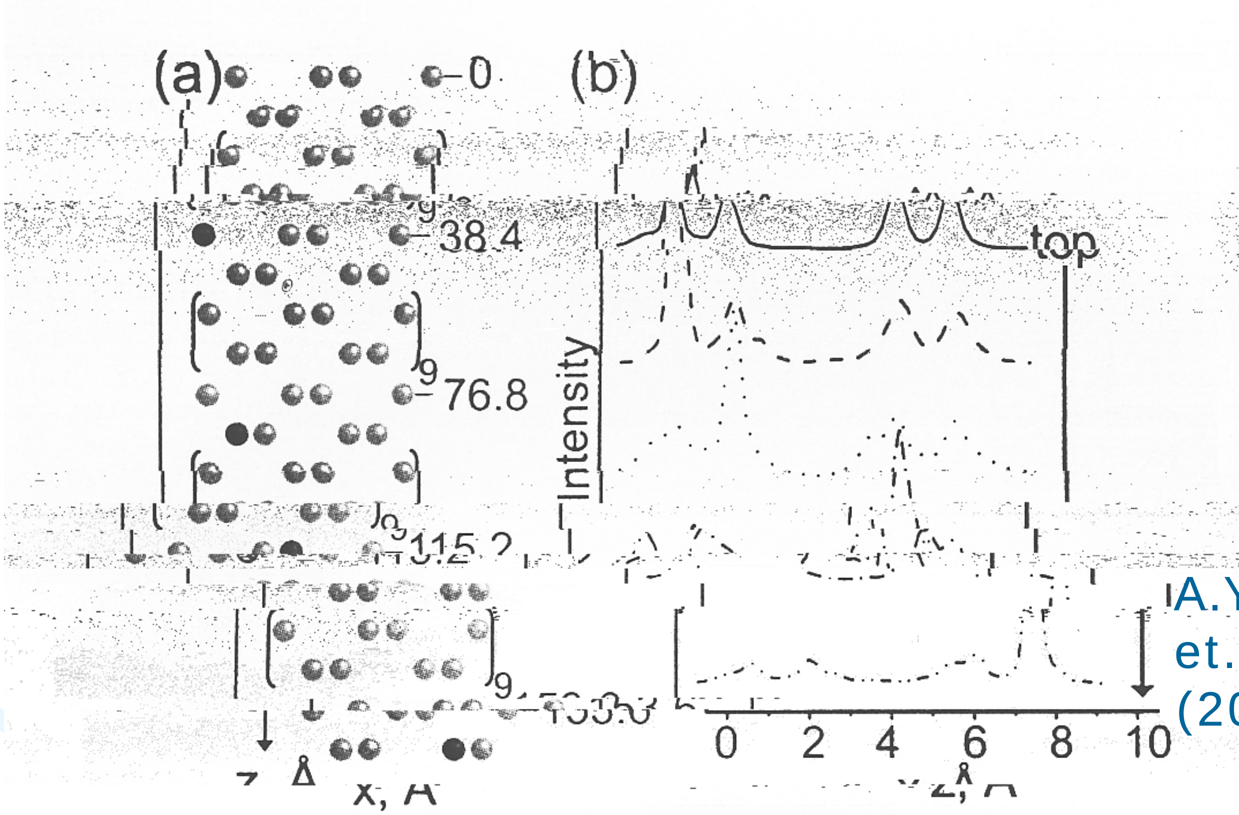

A.Y.Borisevich et.al:J.EM, (2006) 55, 7.

...oped Si crystal with four Bi atoms at different ...ay); (b) simulated HAADF image intensity ...ree probe with 35 mrad semiangle, detector ...d. Defocus varies from 0 (top) to 38.4, 76.8, ...cutively.

Fig. 3 (a) The model d... depths (Bi, black; Si, gr... scans for an aberration-f... angle from 70 to 300 mra... 115.2 and 153.6 Å, conse...

- Cs
Cs f Sin

TEAM FEI 0.5 Å
-achromatic -aplanatic
Achroplanat Cc/Cs
[M.Haider, H.Muller, S.Uhlemann, J.Zach, U.Loebau, and R.Hoeschen: Ultramicroscopy 108 (2008) 167] 1 Cc/Cs
200KV

2
1

Sub-ev-Sub-Å Microscope

H.H.Rose: Sci. Tech. Adv. Mat., 9 (1008) `14107 (30pp).

2008/12/5

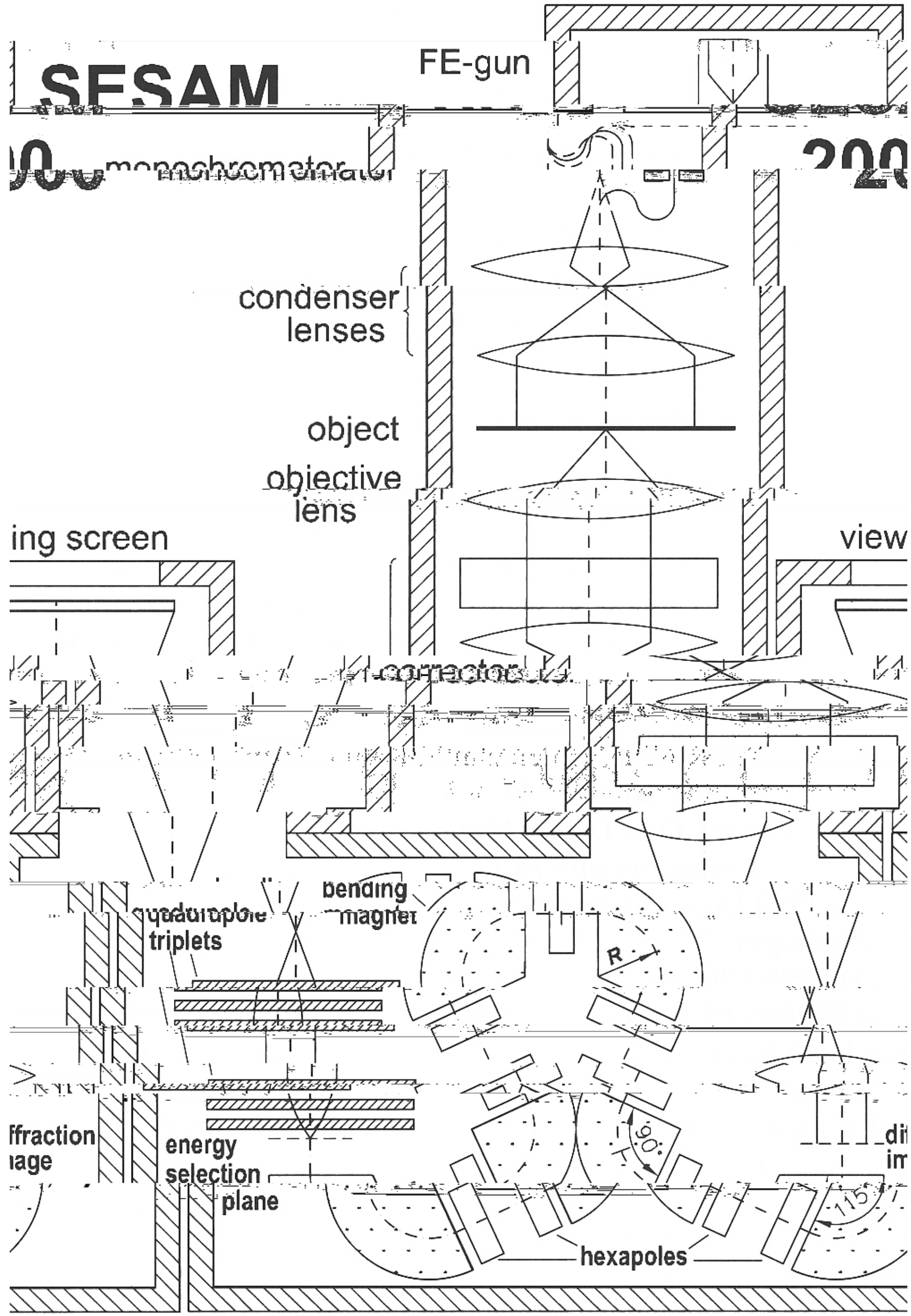

STEM-2008-NION